Engineering Structures 303 (2024) 117522

Contents lists available at ScienceDirect

Engineering Structures

journal homepage: www.elsevier.com/locate/engstruct

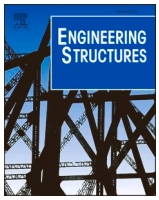

Multi-hazard design of low-damage high-rise steel–timber buildings subjected to wind and earthquake loading

Micol Ciabattoni, Francesco Petrini *, Stefano Pampanin

Department of Structural and Geotechnical Engineering, Sapienza University of Rome, Italy

ARTICLE INFO

Keywords:
Multi-Hazard
Tall buildings
Steel
Laminated timber
Hybrid rocking-dissipative connections
Unbonded post-tensioning
Pres-Lam
Earthquake
Wind
Direct Displacement Based Design

ABSTRACT

This work focuses on the design trade-off aspects related to the structural behavior of tall buildings subjected to the actions of wind and earthquake and on the feasibility of adopting innovative low-damage structural systems and connections combining engineered wood and steel. A multi-hazard approach is developed and proposed, through the use of an efficient equivalent baseline reference to compare the structural performance under two independent whilst competing hazards. Following a capacity-vs-demand approach an Acceleration Displacement Response Spectrum (ADRS) domain, well established in the earthquake engineering environment, is suggested to be extended and adapted to wind design. The innovative procedure is developed and implemented with reference to two case study tall buildings, 18 storey and 36 storey high, respectively. The use of either traditional steel-only connections or innovative low-damage steel-timber hybrid - unbonded post-tensioned rocking-dissipative – connections are employed and compared. Two difference constructions sites are considered: 1) a high seismicity and low wind zone and 2) low seismicity and high wind zone. A Direct Displacement Based Design (DBDD) procedure is firstly implemented to design the structural system targeting the desired level of seismic performance. Then the effects of wind loading are estimated through the analytical procedure provided by the Italian National Research Council (CNR), which allows to calculate wind-induced forces and peak floor accelerations. Peak interstorey drifts are selected as seismic performance indicator, while peak floor accelerations are selected as wind performance indicator with the intent to focus on the building occupants' comfort serviceability limit state. The predicted structural performances are then numerically validated through time series/history analyses under earthquake and wind loading with a lumped plasticity global model of the case-study buildings. Finally, the structural responses under the two actions are compared within the proposed innovative common baseline ADRS domain, allowing to establish the governing design hazard depending on the intensity levels and adopted return periods. Based on these developments, a true multi-hazard approach is proposed for the preliminary design phase of a building subjected to wind and earthquake loading.

1. Introduction

Due to the growth of population density and the increasing of the level of urbanization, in recent decades, there has been a significant development of tall buildings worldwide. In parallel, innovative structural systems in engineered wood – laminated timber - have been introduced in the seismic design of tall timber buildings with the aim of increasing their seismic safety and performance [1]. The most common and emerging types of engineered wood used in the construction of modern buildings are the Glued Laminated Timber (GluLam), the Laminated Veneer Lumber (LVL) and the Cross-Laminated Timber (Cross-Lam, or X-Lam, or CLT). All of them consist of wood slim layers (40–50 mm or 3 mm veneer) glued together (either uni-directionally or alternating parallel and perpendicular to grain boards, respectively) to the assembly of beam elements. Laminated Timber solutions maintain the structural and sustainability qualities of natural wood with a significant reduction of the geometrical and continuity imperfections, leading to significant increase in the mechanical properties of the resulting element (e.g. strength and E-modulus parallel to grain). One of the main perceived drawback (or, better, prejudice) of the use of wood as structural material in seismic regions is arguably related to its limited ductility, something that potentially limits its wider implementation in seismic-resistant structures unless adequate connection solutions and details are implemented. In this context, in recent years

* Corresponding author.
E-mail address: francesco.petrini@uniroma1.it (F. Petrini).

https://doi.org/10.1016/j.engstruct.2024.117522
Received 23 September 2023; Received in revised form 18 December 2023; Accepted 9 January 2024
Available online 28 January 2024

high-performance low-damage technologies have been developed with the goal of minimizing the structural earthquake-induced damage. Starting from the development of PRESSS-technology since the late '90s for precast concrete structures [2,3] these advanced solutions were extended and adapted to engineered wood structural elements and systems, opening new perspective for the extensive use of timber as a sustainable material in the design of multi-storey open-space buildings. Such hybrid rocking-dissipative connections (beam-to-column, column/wall-to foundation) rely on the combined use of unbonded post-tensioned tendons/bars and dissipative elements in the form of internal mild steel bars or external and replaceable "Plug&Play" dissipaters [4]. The unbonded post-tensioned tendons/bars act as an elastic spring providing a fundamental self-centering capability to restore the structure to its pre-earthquake undeformed position with no residual/permanent deformations and negligible damage to the structural elements [5].

In addition, the internal mild steel (Fig. 1a) or external replaceable "Plug&Play" dissipaters (Fig. 1b,c) provide a significant energy dissipation capacity, reducing the overall deformation/displacement/drift of the structure.

The typical moment-rotation behavior of a hybrid connections, associated to this peculiar self-centering and dissipative mechanism, is referred to as "flag-shape" (Fig. 2). The hysteretic area of the loop depends on the ratio between the (re-centering) moment contribution provided by the post-tensioned cable and the (dissipative) one provided by the dissipative devices: the higher this ratio, the smaller the area (and thus the dissipation capability) of the cycle.

Up to now, the implementation of engineered wood elements to replace floor beams in steel buildings, in combination with hybrid rocking-dissipative unbonded post-tensioned connections, has been limited to low-rise buildings, and their design has been mainly developed in the field of earthquake engineering [8]. Furthermore, the introduction of such type of advanced structural connections and systems have prompted a suggests a change in the seismic design philosophy. In fact, current best practices in seismic design of ordinary structures, are based on the human life protection (Life Safety) with secondary importance given to the repair- and service interruption-costs. In a more advanced and comprehensive performance-based design philosophy instead, it is essential to limit the damage to both structural and non-structural elements and control the structural displacement/interstorey drifts which can compromise the serviceability/operational state of the building. This can be achieved by the combined adoption of low-damage technologies, on one hand, and a Direct Displacement Based Design (DDBD) procedure [9] on the other hand, that allows to design structures targeting desired level of displacement performance Given the rocking-dissipative mechanisms of unbonded post-tensioned low-damage systems a displacement-based design procedure is also inherently and particularly suitable to control the behavior of the connections and overall systems.

This paper gives a contribution in the direction of extending the application of engineered wood elements in combination with hybrid jointed ductile connections to mid-rise and tall buildings located in earthquakes and wind-prone areas. Focus will be given to the use of hybrid low-damage steel column and timber beams rocking dissipating connections, through the use of unbonded post-tensioned tendons/bars through the beam-column interface. A framework for a multi-hazard performance-based design considering both wind and seismic performance criteria and objectives is developed and proposed.

Assessing the effects of the wind in the design of tall structures is crucial because, as the height of the building increases, the relevance of the effects induced by the wind increases as well [10], as depicted in Fig. 3. Usually, the main design issue for slender (mainly made in steel) tall buildings under wind is related with the excessive wind-induced floor accelerations [11], that can cause discomfort to the building occupants. As a result, the Serviceability Limit State (SLS) performance criteria tend to govern the design when compared to those related to the Ultimate Limit State (ULS). The design guidelines "CNR-DT 207 R1/2018″ [12], published by the Italian National Research Council, provides a procedure to estimate the peak floor accelerations and their associated limit values not to be exceeded in order to ensure the comfort of the occupants of tall buildings. As shown in Fig. 3, when the fundamental frequency of the building falls in a range where the spectral magnitudes of wind and earthquake are comparable, a trade-off between design configurations as independently driven by the two hazards is necessary.

In this paper, the structural response of steel–timber buildings adopting unbonded post-tensioned rocking/dissipating hybrid connections, when subjected to wind and earthquake loading, is investigated and compared with the response of an equivalent (same floor plan and height) steel buildings with more traditional connections (benchmark). Two case study buildings are selected: a mid-rise (18 storeys) and a high-rise (36 storeys) ones, with a square plan. The two above-mentioned DDBD and CNR approaches are used for the preliminary design of the buildings under earthquake and wind, respectively. Both methods lead to hazard-intensity dependent design solutions, meaning that the design configuration reached by the DDBD and the CNR methods is dependent on the construction site seismic and wind hazards, respectively. By carrying out the design of the two building in different sites (e.g., high seismicity and low-intensity winds, or low seismicity and high winds), the preliminary sizing of the structural elements is first developed by considering vertical and seismic loads, and then the performance under wind loads is assessed. The effectiveness of this integrated design procedure is validated through non-linear dynamic analyses: 12 natural (i.e. recorded ground motions) seismic signals are selected and scaled to be

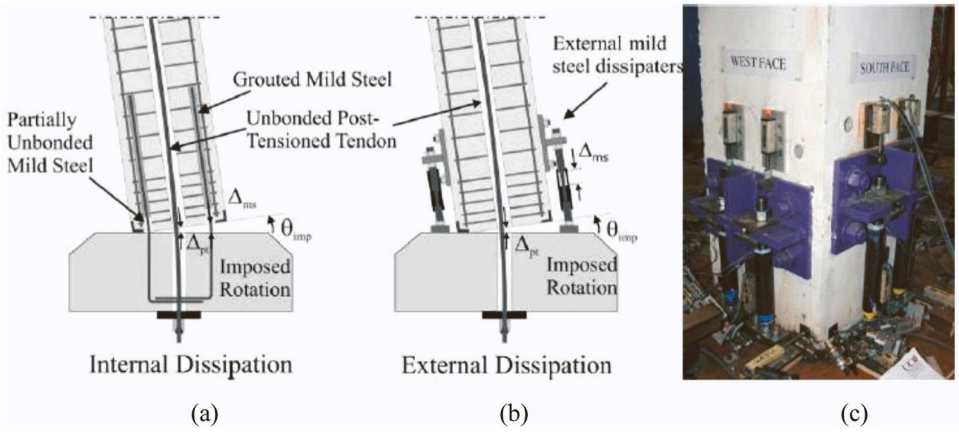

Fig. 1. Internal (a) versus external (b), (c) replaceable dissipaters/fuses at the base-column pier connection (after [6]).

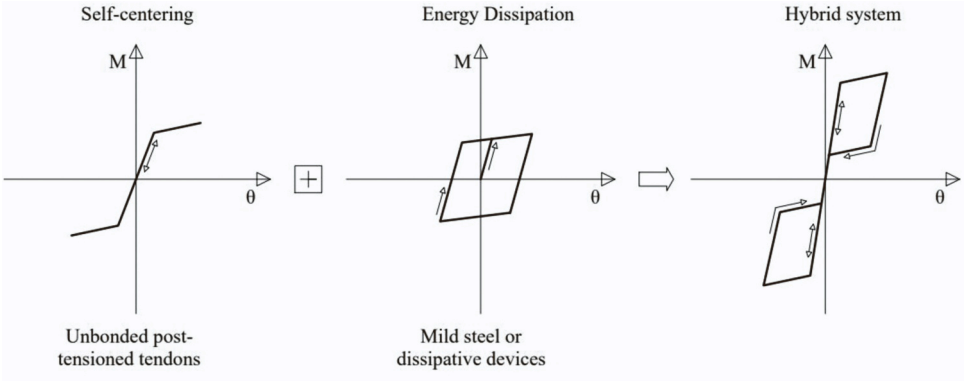

Fig. 2. Typical moment-rotation "flag-shape" hysteretic behavior of hybrid connections (modified after [7]).

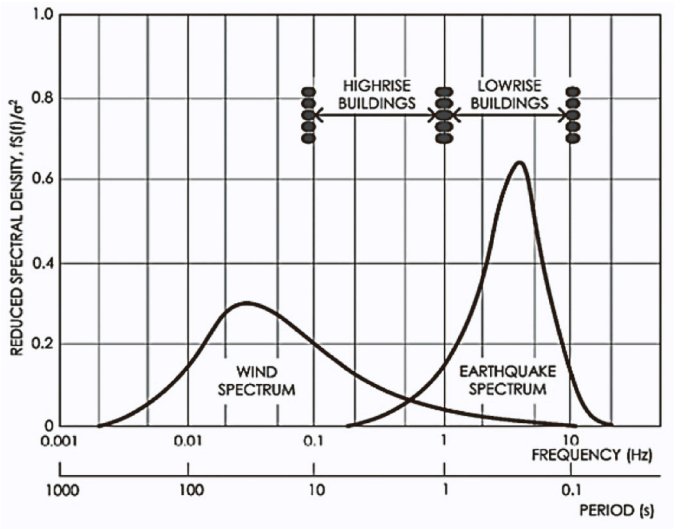

Fig. 3. Frequency range of structures excited by wind and earthquake (after [10]).

compatible with site-dependent design-level earthquake spectra in each case, while 12 sets of turbulent wind forces time series are numerically generated starting from the wind turbulence spectra compatible with the selected sites and depending on the aerodynamic of the structure.

As specified in Petrini et al. [13], and by others [14], when dealing with these type of structural design scenarios, there are a number of issues to be addressed in order to obtain a true multi-hazard design. One of these issues concerns the so called "unified framework problem": different hazards should be treated by a common language and common frameworks to efficiently compare their effects in the analysis of the performances panorama (see also [1]). In this view, the performances of the different case-study structures under the two hazards are compared within the so-called ADRS (Acceleration Displacement Response Spectrum) domain, commonly used in earthquake engineering studies. This allows to understand what hazard is dominant for the building performances on a case-by-case basis. The extension of the ADRS method to wind engineering problems is the second original contribution provided by this paper. Then the ADRS comparison method is used for proposing some true multi-hazard design considerations.

Section 2 provide the description and implementation of the DDBD and CNR performance-based design approaches, adopted in this study. In Section 3 the performances of innovative relatively tall steel-timber buildings equipped with hybrid connections are analyzed under wind loading. In the final Section 4, multi-hazard design considerations are developed by considering two independent (but competing) hazards for such kind of structures, with the effort of developing and proposing an approach to compare the different hazards by using a common language, in turns leading to the extension and implementation of the ADRS capacity spectrum approach to wind engineering.

2. Performances based design methods under single hazards

2.1. Direct displacement based design (DDBD) for earthquakes

The fundamental concept behind the DDBD [2,9] is that structures should be designed to achieve a target level of performance, defined by a limit drift (or ductility, rotation, deformation), under a specific level of seismic intensity. A displacement spectrum is used (entering with the target displacement) instead of a more typical acceleration spectrum. The multi-degree-of-freedom (MDOF) structure is converted into an equivalent single degree of freedom (SDOF) system, characterized by the secant stiffness at the target design displacement and by an (Area-based) equivalent viscous damping, given by the combination of the elastic damping and hysteretic energy absorbed during the inelastic response.

The three key parameters of the SDOF system, namely Target/Design displacement, Δ_d, the Effective Mass, m_e and the Effective Height, H_e, are derived as follows:

$$\Delta_d = \frac{\sum_{i=1}^{n}(m_i\Delta_i^2)}{\sum_{i=1}^{n}(m_i\Delta_i)} \tag{1}$$

$$m_e = \frac{\sum_{i=1}^{n}(m_i\Delta_i)}{\Delta_d} \tag{2}$$

$$H_e = \frac{\sum_{i=1}^{n}(m_i\Delta_i H_i)}{\sum_{i=1}^{n}(m_i\Delta_i)} \tag{3}$$

where m_i, Δ_i and H_i are the i^{th} storey mass, the displacement profile and the height for the storey "i" respectively, and "n" is the number of storeys of the building. For tall buildings, as the fully dynamic response is the sum of the response of each mode, a SDOF representation underestimates the base shear and thus section demands in the structure. So, during the DDBD procedure, the allowable design displacements are reduced by the higher mode effects reduction factor, ω_θ (with ω_θ =1.15–0.0034 H_{tot} from Priestley et al. [9]). This reduction takes into account the excepted increased deformations of the system at the design level due to additional higher mode forces neglected in the SDOF approximation.

The target/design intersorey drift at the critical floor θ_d is the starting point of the DDBD approach and is selected by the designer in

accordance with the desired/acceptable level of performance. The design drift θ_d can be expressed as the sum of an elastic drift θ_y component and a plastic drift $\theta \boldsymbol{p}$.

The equivalent viscous damping, ξ, can be estimated depending on the design displacement ductility, μ_Δ, of the system [9,15–17]). Since the latter is directly linked to the yield displacement, Δ_y, the correct definition of the displacement profile of the structure under lateral forces (e.g. by a non-linear static analysis) is essential. Then the evaluation of the damping allows to reduce the seismic displacement design spectrum through a damping-based reduction factor in order to obtain the effective period of the system, T_{eff}. The period T_{eff} is fundamental for the estimation of the effective design stiffness K_{eff}, (Eq. 4), the base shear (V_b) and the floor forces that will be applied along the height of the structure.

$$K_{eff} = \frac{4 \bullet \pi^2 \bullet m_e}{T_{eff}} \tag{4}$$

The key steps of the DDBD approach are shown in Fig. 4. The base shear *Vb* obtained at the last step of the flowchart can be used together with the displacement profile of the building in order to trace back the floor shear at the different building heights and then to design the building columns and the beam-columns connections.

2.2. Users' comfort based design for wind

The CNR-DT 207 R1/2018 [12] guidelines, provides within a single document the key principles and rules necessary for an engineer to study the behavior of buildings under wind actions in a preliminary design phase.

Usually the wind-resistant structural design of low-damped mid- and high-rise buildings is driven by the comfort performances requirements for the building occupants. It is recognized that excessive floor accelerations can induce discomfort in building' occupants [11], with consequent activity disruption. It is thus fundamental to estimate the value of the along-wind, across-wind and torsional accelerations at the center of torsion of the upper floors of the building, associated with the average wind speed with return period of 1 year or 10 years [19]. The designer should verify that the values of along-wind and across-wind peak accelerations remain below certain perception thresholds a_l. The latter thresholds are related to the dominant vibration frequency in each main vibration direction (also referring to the mean wind direction or orthogonally to it as along- or across-wind), which is often taken equal to first vibration natural frequency of the structure (n_0) along the investigated direction. The vibration thresholds are also related to the intended use of the building (apartments or offices) as expressed in Eq. (5) and shown in Fig. 5.

$$a_l = \begin{cases} \frac{a_0}{n_0^{0.56}} \text{for} n_0 < 1Hz \\ a_0 \text{for} 1Hz \le n_0 \le 2Hz \\ 0.5 \bullet a_0 \bullet n_0 \text{for} n_0 \ge 2Hz \end{cases} \tag{5}$$

where:

a_0 is the peak acceleration reference value, taken as 6 cm/s^2 for office buildings and 4 cm/s^2 for residential buildings;.

n_0 is the dominant oscillation frequency (taken as the first natural frequency of the building in the considered direction).

The peak accelerations experienced by the building under the design wind depend on the characteristics of the incident wind and the dynamic and aerodynamic properties of the building. The CNR-DT 207 R1/2018 [12] provides an analytical approach to allow the designer the estimation of the peak accelerations experienced by tall buildings at the top floor under the design wind. When the peak acceleration values are higher than the recommended limit (Fig. 5), it is necessary to increase the damping of the system either by adding supplemental vibration control devices, or by changing the building design.

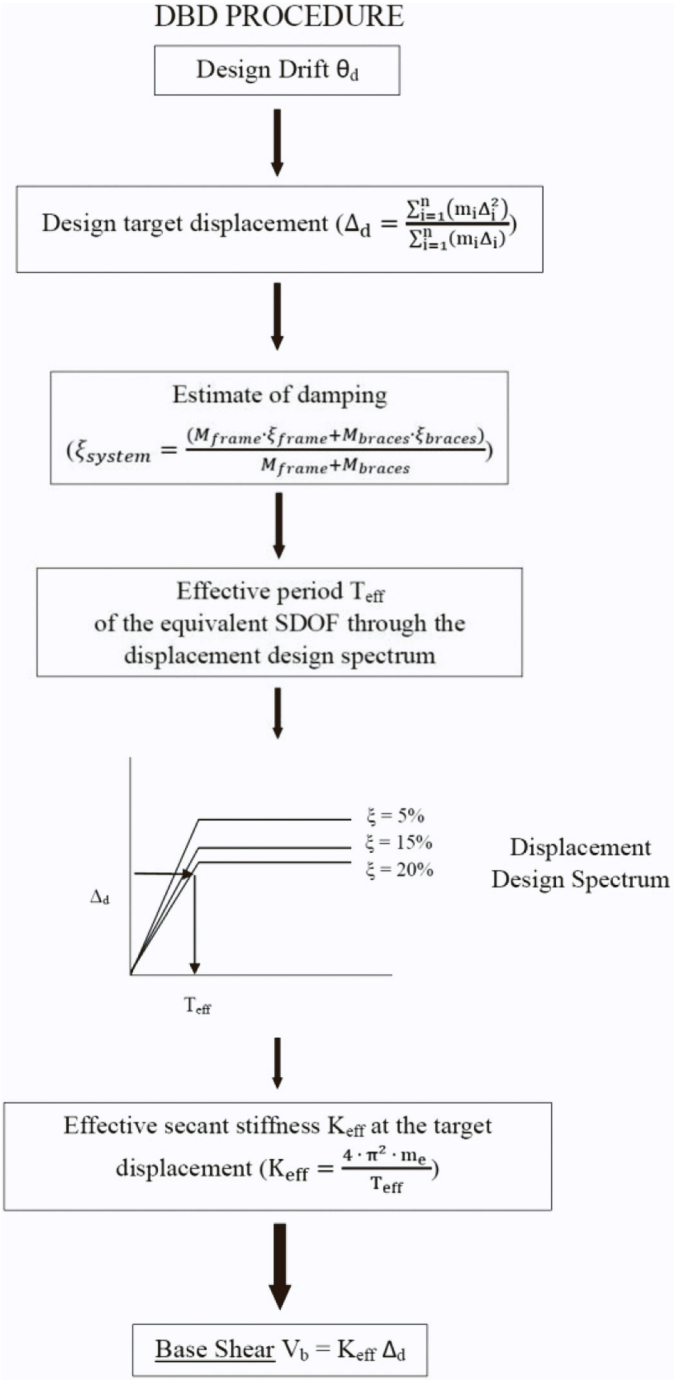

Fig. 4. DDBD procedure (modified after [18]). Meaning of symbols is specified in the main text.

The peak acceleration in the across-wind direction (most-critical one for square-plan tall buildings shown in Fig. 6) is evaluated as:

$$a_{aL}(z) = g_L \bullet \sigma_{aL}(z) \tag{6}$$

where:

g_L is the across-wind peak factor (Eq. 8);.

σ_{aL} is the standard deviation of the across-wind acceleration at height z:

$$\sigma_{aL}(z) = \frac{0.5 \bullet \rho \bullet v_m^2(h) \bullet b \bullet h}{m_L} C_L \bullet R_L \bullet \Phi_L(h) \bullet \Phi_L(z) \tag{7}$$

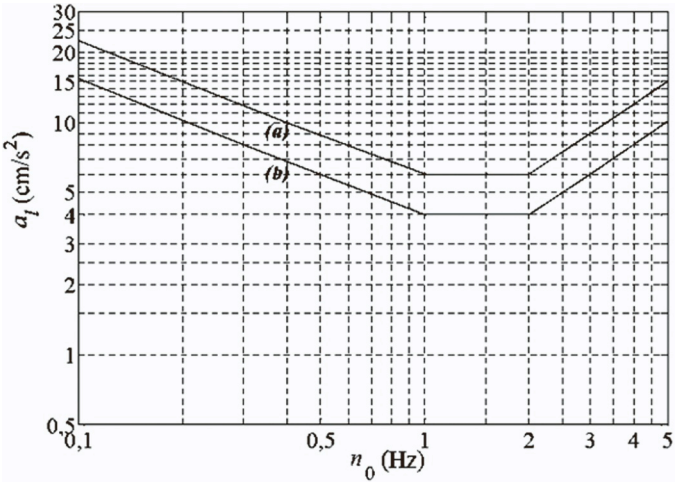

Fig. 5. Perception thresholds in terms of peak acceleration values for office as a function of the dominant oscillation frequency (a) and residential buildings (b) (after CNR 2018).

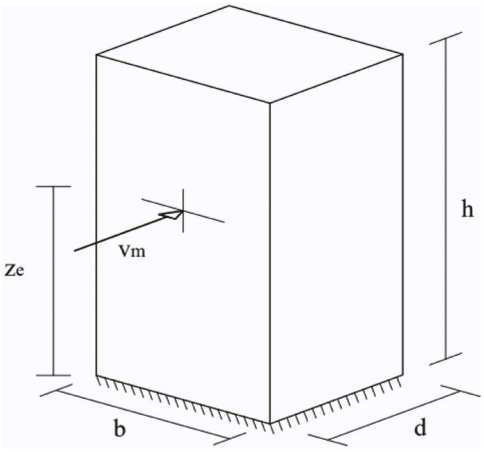

Fig. 6. Rectangular plan tall building (modified after CNR 2018 [12]).

where:

ρ is the air density (1.25 kg/m^3);.

$v_m(h)$ is the mean wind velocity, evaluated at z = h, for a design return period T_R suitable for habitability assessment;.

b is the building width;.

h is the building height;.

m_L is the generalized mass related to the building first vibration mode;.

C_L is the aerodynamic force coefficient;.

R_L is the across-wind resonant response factor (Eq. 9);.

$\Phi_L(z)$ is the first across-wind mode shape.

$$g_L = \sqrt{2 \bullet \ln(n_L \bullet T)} + \frac{0.5772}{\sqrt{2 \bullet \ln(n_L \bullet T)}} \geq 3 \tag{8}$$

where:

n_L is the fundamental across-wind eigen-frequency of the building;.

T is the mean wind velocity averaging time interval, $T = 600$ s

$$R_L = \frac{\pi \bullet S_L}{4 \bullet \xi_L} \tag{9}$$

$$S_L = \sum_{j=1}^{m} \frac{4k_j \bullet (1 + 0.6 \bullet \beta_j) \bullet \beta_j}{\pi} \quad \frac{\left(\frac{n_L}{n_{sj}}\right)^2}{\left[1 - \left(\frac{n_L}{n_{sj}}\right)^2\right]^2 + 4 \bullet \beta_j^2 \bullet \left(\frac{n_L}{n_{sj}}\right)^2} \tag{10}$$

$$m = \begin{cases} 1 d/b < 3 \\ 2 d/b \geq 3 \end{cases} \tag{11}$$

d is the side size of the building

$$k_1 = 0.85 \tag{12}$$

$$k_2 = 0.02 \tag{13}$$

$$\beta_1 = \frac{\left(\frac{d}{b}\right)^4 + 2.3 \bullet \left(\frac{d}{b}\right)^2}{\left[2.4 \bullet \left(\frac{d}{b}\right)^4 - 9.2 \bullet \left(\frac{d}{b}\right)^3 + 18 \bullet \left(\frac{d}{b}\right)^2 + \left(\frac{d}{b}\right) - 0.15\right]} + \frac{0.12}{\left(\frac{d}{b}\right)} \tag{14}$$

$$\beta_2 = 0.28 \bullet \left(\frac{d}{b}\right)^{-0.34} \tag{15}$$

$$n_{s1} = \frac{0.12}{\left\{1 + 0.38 \bullet \left(\frac{d}{b}\right)^2\right\}^{0.89}} \frac{\mathrm{v_m(h)}}{\mathrm{b}} \tag{16}$$

$$n_{s2} = \frac{0.56}{\left(\frac{d}{b}\right)^{0.86}} \frac{v_m(h)}{b} \tag{17}$$

where:

ξ_L is the damping ratio in the first across-wind mode;.

$v_m(h)$ is the mean velocity, evaluated at height $z = h$;.

β_1, β_2 are dimensionless coefficients (Eqs. 14 - 15);.

n_{s1}, n_{s2} are dimensionless parameters (Eqs. 16 - 17);.

If not evaluated by a modal analysis of the building, the fundamental across-wind natural frequency of the building n_L used for evaluating both the peak acceleration (Eq. 8) and the perception thresholds (Eq. 5), can be preliminary evaluated within a range suggested by the CNR and depending on the examined case:

$$n_L = \frac{1}{0.024 \bullet h} \div \frac{1}{0.020 \bullet h} \text{for steel buildings} \tag{18}$$

$$n_L = \frac{1}{0.015 \bullet h} \div \frac{1}{0.012 \bullet h} \quad \text{for steel–timber buildings with more rigid connections} \tag{19}$$

The lower bounds of the frequencies range are used for the ultimate limit state checks, while the upper bounds are valid for the habitability checks.

3. Performances of steel and steel-timber buildings with different heights

In this section, the above-mentioned analysis methods are applied for the performance assessment of some case study buildings under wind and earthquake loading.

The four case studies analyzed consist of two mid-rise buildings (18 storeys) and two tall buildings (36 storeys). All four structures are regular in both plan and height, made by seismic-resistant frame system, while in the central part of the plan they have a brace core with "Buckling Restrained Brace" (BRB) braces. Two of the four case studies (one with 18 storeys and the other with 36 storeys) are made entirely of S355 steel, while the other two have steel columns and braces while the beams are made of engineered wood. It is in the two buildings with timber beams that the hybrid unbonded post-tensioned connections described in the previous sections are introduced.

The buildings are modeled in the SAP2000® FE commercial code, and their structural members are pre-sized under vertical loads. Then the hybrid beam-column connections (with "Plug&Play" dissipaters) of the steel-timber buildings are sized by applying the DDBD procedure. The performances of the case-study prototype buildings are then assessed by applying nonlinear time history analyses under earthquake

loading and the simplified CNR procedure plus nonlinear time history analysis under wind loading. The goal of the section is twofold:

i) testing the efficiency of the DDBD and of the CNR procedures in designing this type of buildings by assessing their performance through non-linear time history analyses and comparing with the targeted design levels;
ii) compare the performance of the two buildings typologies (steel or steel-timber with hybrid unbonded post-tensioned connections) under the two hazards when applied separately; also investigate the influence of various level of seismic or wind hazard intensities associated to the construction site.

The performance analyses are carried out for the case-study buildings both at the serviceability limit state (SLS) and at the ultimate limit state (ULS). The SLS corresponds to the damage limit state for a return period $T_R = 101$ years for the earthquake and to the occupants' comfort limit state for a TR= 10 years for the wind, while the ULS corresponds to the life safety for the earthquake (T_R=949 years) and to "linear elastic operational condition" with TR= 100 years for the wind [19].

This approach, implying the definition of an initial design configuration by considering a single hazard (e.g. earthquake for the hybrid low-damage connections) and then the check of the performances of that configuration under another hazard (e.g. wind) represents the traditional design approach carried out in current practice [20,21]. Furthermore, an alternative and improved integrated design procedure to pre-size the building configuration and structural systems/elements, following a multi-hazard approach (earthquake plus wind) will be proposed in Section 4.

3.1. Description of the buildings, construction sites and FE modeling

The first two case studies consist of 18-storey, three (7.35 m long) bays buildings, with regular configuration in plan and elevation, relying upon a central core with Buckling Restrained Braces (BRBs) and perimeter frames. In the first building configuration (Fig. 7) the perimeter frame connections consist of traditional shear-resisting steel bolted connection, while in the second building configuration hybrid steel-timber low-damage solutions are adopted, consisting of steel columns connected to GluLam engineered wood beams through unbonded post-tensioned tendons/bars and external replaceable Plug&Play dissipation devices.

The BRBs [22] consists of a central steel core, its bond-preventing layer and its casing. The steel core is designed to resist the full axial force developed in the bracing, the bond-preventing layers decouples the core from the casing, which through its flexural rigidity, provides lateral support against the buckling of the steel core element. The latter is typically made of concrete-filled steel tubes. Because BRBs achieve a high level of ductility, they can absorb significant amount of energy during cyclic loadings, thus, the interstorey drifts as well as the seismic internal actions (moment, shear, axial load) applied to the structure is efficiently reduced.

For each considered limit state "LS", the peak ground acceleration (PGA_{LS}) and the mean wind speed at sea level ($V_{m\text{-}LS}$) are taken as intensity measures for earthquakes and winds, respectively. Two different construction sites are then considered for each building, namely a high-seismicity and moderate-wind ($PGA_{SLS} = 0.406$ g; $V_{m\text{-}SLS} = 25.0$ m/s), and a low-seismicity and high-wind ($PGA_{SLS} = 0.182$ g; $V_{m\text{-}SLS}$= 30.0 m/s) region.

The same pre-design and investigation has then been carried out for two additional 36 storey (total height of 126 m and plan area of 25.5 m x 25.5 m) configurations with same structural schemes and same connection typologies. For all the four building configurations the floor slabs consist of a composite concrete-steel solution, with corrugated metal sheets and a 15 cm thick concrete slab.

All the case study buildings have been modeled in SAP2000® Finite Element code by using a lumped plasticity approach with linear-beam elements and rotational springs/links at the rocking-dissipative interface. Modal linear dynamic (response spectrum) analysis and time-history analyses are carried out to confirm the results obtained with the simplified DDBD and CNR design methods described above. In the numerical model, both material and geometric (associated to the rocking mechanism) non-linearity are accounted for by adopting a lumped plasticity approach.

The BRBs have been modeled by using multilinear plastic links of BRB Hardening type [23].

Concerning the steel buildings, in accordance with the Capacity Design method, aimed at maximizing the building ductility, while protecting from brittle local and global mechanism, the formation of axial plastic hinges is expected in bracing members, while combined axial-bending plastic hinges are expected in columns (especially at the base). On the contrary, for this configuration, bending plastic hinges are not expected in the beams since they do not contribute to the lateral structural response.

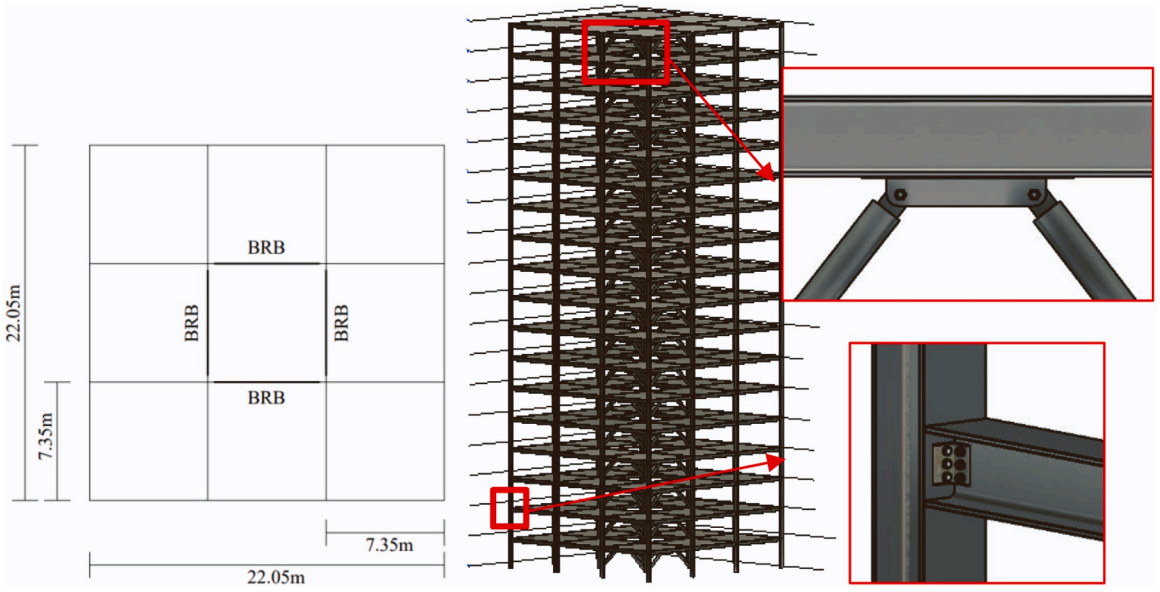

Fig. 7. 18-storey case-study building with traditional bolted connection (the connections shown refer to the X and Y directions).

In the low-damage timber – steel buildings (Fig. 8), the hybrid connections are modeled as two links (moment-rotational springs) in parallel with proper hysteretic rules: the first one is non-linear elastic to represent the self-centering behavior of the unbonded post-tensioned tendons, while the second one is elastoplastic with hardening to represent the dissipative contribution of the Plug&Play devices.

In Table 1, the main characteristics of the structural elements representing the FEM model are reported.

3.2. Pre-sizing of the case study buildings

The structural elements of the case study buildings have been presized to satisfy specific checks requirements under vertical permanent and variable loads (the latter ones taken equal to 30% of the full load scenario). The non-structural weights include the internal partitions, the facades, the screed, the services, and the ceiling. The following accidental loads are considered as classified by the Italian Standards for structural design NTC2018: an anthropic load corresponding to the service category B1 (offices closed to general public), an anthropic load corresponding to the service category H (roof accessible only for maintenance and repair) for the roof slab and the snow load.

The values of the loads considered in the analyses are reported in Tables 2 and 3:

The aforementioned loads have been applied according to the combination rules specified by the Italian Standards for structural design NTC2018 at paragraph 2.5.3.

As regards the beams, a section height equal to 1/20 of the span has been initially assumed and then checked against bending, shear and deformability requirements.

Based on the aforementioned loads, the column section has been also selected and checked against compression failure and Euler instability mechanism by considering a reduced capacity equal to 30% of the full Eulerian buckling load.

Since the total axial load acting on the columns decreases with the height above the ground, the size of the columns reduces every 6 floors for case study buildings with 18 floors and every 12 floors for 36 storeys case study buildings.

As regards the central part of the buildings, it is made up of the BRBs which have been entrusted with 50% of the resistance to seismic loads (the remaining 50% is assigned to the perimeter frames). As explained in the previous sections, they have been designed such that the central core absorbs the full axial force with the external casing contrasting the buckling. The behavior of these elements is characterized by stable and repeatable hysteresis cycles, which allow the structure to reach a high level of ductility and dissipate a significant amount of energy [22,24,25].

Table 1
main characteristics of FEM model elements.

Steel columns and steel beams	
Elastic Modulus (MPa)	210 000
Shear Modulus (MPa)	80 770
Yield strength (MPa)	355
Ultimate strength (MPa)	510
Specific weight (kg/m^3)	7850
GluLam engineered wood beams	
Elastic Modulus, parallel (MPa)	14 700
Bending strength (MPa)	36
Tension strength, parallel (MPa)	26
Compression strength, parallel (MPa)	31
Shear strength (MPa)	4.3
Tension strength, perpendicular (MPa)	0.6
Compression strength, perpendicular (MPa)	3.6
Elastic Modulus, perpndicular (MPa)	490
Specific weight (kg/m^3)	450
Shear Modulus (MPa)	910
Braces	
Type Link	MultiLinear Plastic
Hysteresis type	BRB Hardening
Hardening factor	1.15
Effective damping	0.02
Unbonded post tensioned tendon	
Type Link	MultiLinear Elastic
Yield strength (MPa)	835
Effective damping	0.02
Plug&Play devices	
Type Link	MultiLinear Plastic
Hysteresis type	Hardening
Effective damping	0.02

The following Fig. 9 illustrates the described behavior of the BRBs.

Regarding the connections, as already mentioned, in the steel building configurations the beams are connected to the columns by means of bolted connections. In this case, for simplicity, the connection elements (bolts and L-shaped plates) have not been explicitly sized. On the other hand, in the timber – steel building configuration the connections are made up of two elements (post-tensioned cable and external dissipaters) whose sizing was actually carried out for each seismic action. For this reason, their characteristics are provided in the next

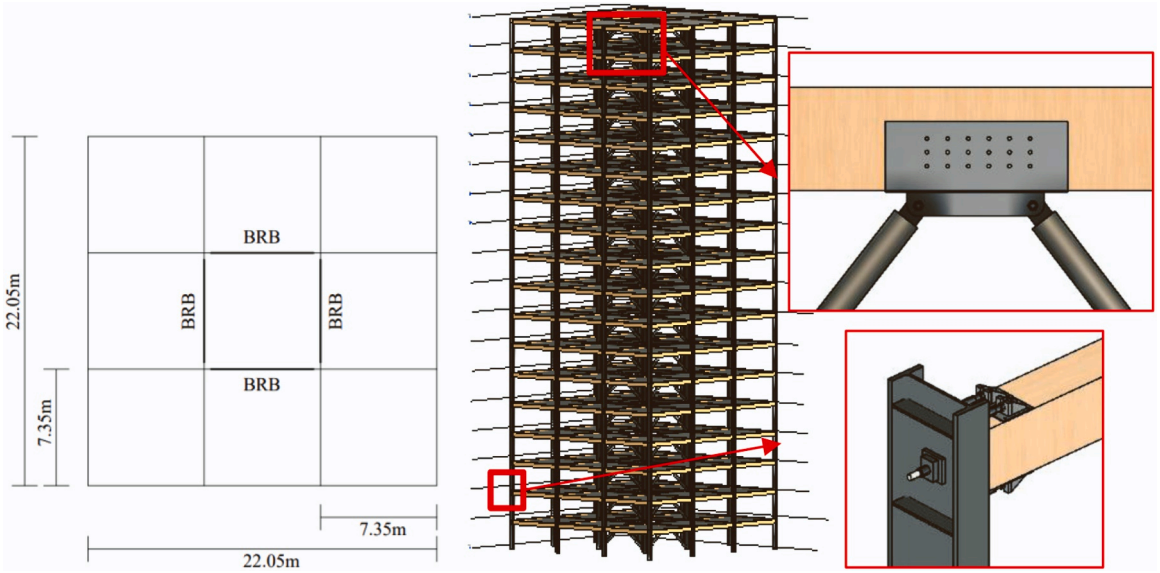

Fig. 8. 18-storey case-study building with hybrid connection (the connections shown refer to the X and Y directions).

Table 2
vertical permanent and variable loads considered in the analyses for the four cases study building at site with high seismicity and low wind.

Site with high seismicity - low wind	18-storyes Steel building	18-storeys Steel-timber building	36-storyes Steel building	36-storeys Steel-timber building
Structural weights G_1 (kN)	1112.83	896.20	3462.15	3108.08
Interstorey slab weight g_2 (kN/m^2)	6.07	6.07	6.07	6.07
Roof slab weight g_2 (kN/m^2)	6.07	6.07	6.07	6.07
Stairs load for interstorey slab q (kN/m^2)	4.00	4.00	4.00	4.00
Anthropic load for interstorey slab q (kN/m^2)	2.00	2.00	2.00	2.00
Anthropic load for roof slab q (kN/m^2)	0.50	0.50	0.50	0.50
Snow load q (kN/m^2)	1.62	1.62	1.62	1.62

Table 3
vertical permanent and variable loads considered in the analyses for the four cases study building at site with low seismicity and high wind.

Site with low seismicity - high wind	18-storyes Steel building	18-storeys Steel-timber building	36-storyes Steel building	36-storeys Steel-timber building
Structural weights G_1 (kN)	1129.38	863.88	3353.25	2818.84
Interstorey slab weight g_2 (kN/m^2)	6.07	6.07	6.07	6.07
Roof slab weight g_2 (kN/m^2)	6.07	6.07	6.07	6.07
Stairs load for interstorey slab q (kN/m^2)	4.00	4.00	4.00	4.00
Anthropic load for interstorey slab q (kN/m^2)	2.00	2.00	2.00	2.00
Anthropic load for roof slab q (kN/m^2)	0.50	0.50	0.50	0.50
Snow load q (kN/m^2)	1.00	1.00	1.00	1.00

section.

3.3. Seismic DDBD and hybrid connections sizing

The seismic design procedure DDBD has been applied to each case study building. The first step was to define the target drift in accordance with the desired level of performance. Subsequently, the MDOF structure has been transformed to an equivalent SDOF system as described in Section 2. In this regard, it has been necessary to assume the displacement profiles: given the combination of a frame system with a braced core, similar to a dual system, it was reasonable to expect a linear profile. A higher mode modification factor ω_d (Eq. 20) for the target displacement has been introduced to take into account the higher mode effects, which can be significant in tall buildings [9]:

$$\omega_d = 1.15 - 0.0034 H_n \tag{20}$$

where H_n is the height of the building (expressed in meters).

Then, the ductility of the structural system (μ_{SYS}) is given by the contribution of the *MRF* and *BRB*s, and its energy dissipation capacity (ξ_{sys}) has been assessed as [26,9,15]:

$$\xi_{sys} = \frac{(M_{MRF} \bullet \xi_{MRF} + M_{BRB} \bullet \xi_{BRB})}{M_{MRF} + M_{BRB}} \tag{21}$$

where:

M_{MRF} is the moment entrusted to the resistant frame system;.

M_{BRB} is the moment entrusted to the resistant BRB system;.

For steel buildings the damping of two resistant systems is evaluated as:

$$\xi_{MRF} = \xi_{steelframe,MRF} - k_{MRF} \bullet (\xi_{conventional} - \xi_{steel}) \tag{22}$$

$$\xi_{BRB} = \xi_{steelframe,BRB} - k_{BRB} \bullet (\xi_{conventional} - \xi_{steel}) \tag{23}$$

$$k_{MRF} = \mu_{MRF}{}^{\lambda} \tag{24}$$

$$k_{BRB} = \mu_{BRB}{}^{\lambda} \tag{25}$$

$$\mu_{MRF} = \frac{\theta_d}{\theta_{yMRF}} \tag{26}$$

$$\mu_{BRB} = \frac{\theta_d}{\theta_{yBRB}} \tag{27}$$

λ is a correction coefficient and it is -0.617;.

θ_d is the target drift;.

θ_y is the yield drift;.

ξ_{steel} is 2%;.

$\xi_{conventional}$ is an elastic damping level, taken equal to 5%;

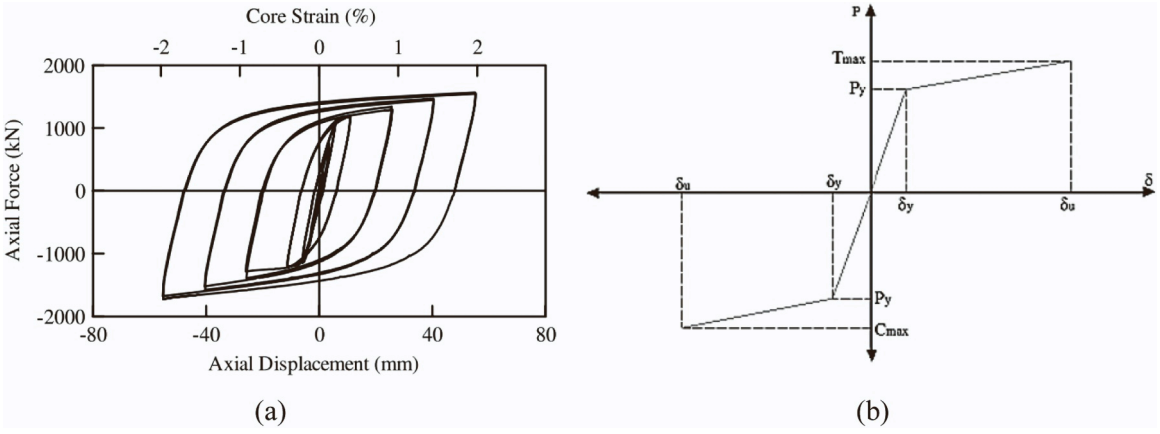

Fig. 9. (a) Representative hysteretic curve for a BRB test specimen (after [24]), (b) bilinear curve force-displacement (right).

$$\xi_{steelframe,MRF} = 0.05 + 0.577\left(\frac{\mu_{MRF} - 1}{\mu_{MRF} \bullet \pi}\right) \quad (28)$$

$$\xi_{steelframe,BRB} = 0.05 + 0.577\left(\frac{\mu_{BRB} - 1}{\mu_{BRB} \bullet \pi}\right) \quad (29)$$

For steel-timber buildings with hybrid connections, the damping of two resistant systems is evaluated as [26,16]:

$$\xi_{MRF} = \xi_{eq,v} + k \bullet \xi_{eq,h,v,MRF} \quad (30)$$

$$\xi_{BRB} = \xi_{eq,v} + k \bullet \xi_{eq,h,v,BRB} \quad (31)$$

$\xi_{eq,v}$ is between 2% and 5%;.

k is a reduction factor used to correct the hysteretic damping (the suggest range is 0.6–1);

$$\xi_{eq,h,v,MRF} = \frac{\beta_F \bullet (\mu_{MRF} - 1)}{\mu_{MRF} \bullet \pi \bullet [1 + r \bullet (\mu_{MRF} - 1)} \quad (32)$$

$$\xi_{eq,h,v,BRB} = \frac{\beta_F \bullet (\mu_{BRB} - 1)}{\mu_{BRB} \bullet \pi \bullet [1 + r \bullet (\mu_{BRB} - 1)} \quad (33)$$

r is a post-yield stiffness ratio between 0.1 and 0.3;.

β_F is the re-centering ratio of the global system (flag loop parameter);.

The estimation of the damping of the structure allowed to calculate the seismic spectral reduction factor η_{m0} [9]

$$\eta_{m0} = \sqrt{\frac{01}{0.05 + \xi sys}} \quad (34)$$

which has been applied to the 5%-damped elastic displacements spectrum to obtain the damped design one. Entering the spectrum with the target displacement, the effective target period is derived and consequently the effective stiffness (Eq. 4) and the base shear (see Fig. 4).

By distributing the base shear along the height of the building, the internal actions in the members (bending moment, shear, axial load) are evaluated and thus the hybrid connections are sized both in terms of post-tensioned tendons/bars (amount, location, unbonded length, initial post-tensioning) and Plug&Play (size, shape, fuse diameters and length) devices [4].

The values of the key DDBD design parameters for the four examined case-study buildings at the two considered construction sites are reported in Tables 1 and 2.

Fig. 10 illustrates the moment-rotation hysteresis (capacity) of a connection for one of the analyzed case study buildings.

3.4. 3.4 Simplified performance analysis under wind

Figs. 11 and 12 show the wind-induced peak acceleration values for the top floor in each case study, obtained for the different sites, at the considered return period TR= 10 years, by following the CNR simplified procedure described in previous Section 2.2. In general, it can be noted that steel buildings are subjected to greater accelerations than the steel-timber counterparts. Across-wind accelerations are assumed to be relevant only for the 36-storey higher buildings and have not been evaluated for the 18-storey cases.

3.5. Time history analyses

Linear Dynamic (response spectrum modal) analysis and Nonlinear Time-History Analysis (NLTHA) have been carried out in order to assess the performances of the alternative design configurations under wind and earthquake loading respectively, and the efficiency of the simplified design/performances analysis methods adopted above. The NLTHA for seismic loading consist of the application of base acceleration time series to the FE model. The time histories were extracted from the archive of the INGV (Italian National Institute of Geology and Vulcanology). Tolerance limits were defined within which the accelerogram may deviate from the reference spectrum (10% below and 30% above).

A total of 12 acceleration input ground motion have been adopted for each considered construction site.

The NLTHA results, derived from the application of the 12 acceleration time series, are presented in terms of maximum interstorey drifts and compared to the target drift values adopted in the DDBD design phase (see Table 4 and Table 5). Interstorey drift results are shown in Fig. 14 and in Fig. 15 for the site with high seismicity. In addition to the response under each single seismic signal, indicated by "THi" (with i = 1,2,…12), the average value and its standard deviations ("sd" in figure) are presented. From the figure, it is clear how nonlinear dynamic analyses show the importance of higher modes, which were not properly

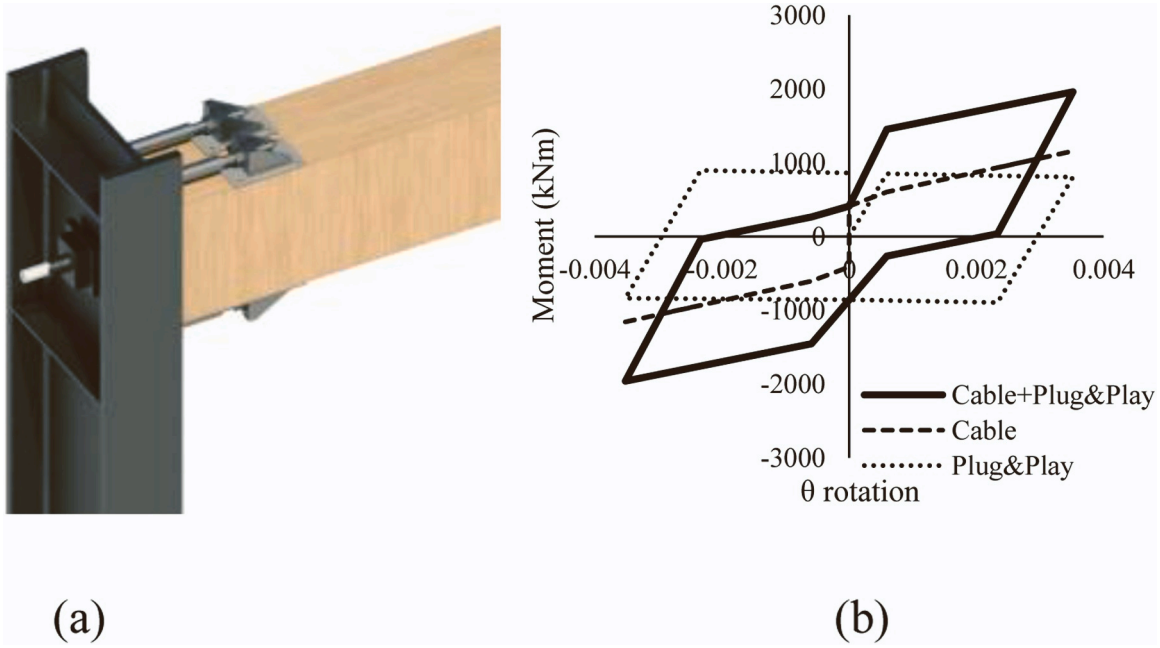

Fig. 10. Hybrid steel-timber post-tensioned connection: (a) morphology; (b) moment-rotation flag-shape hysteresis behavior.

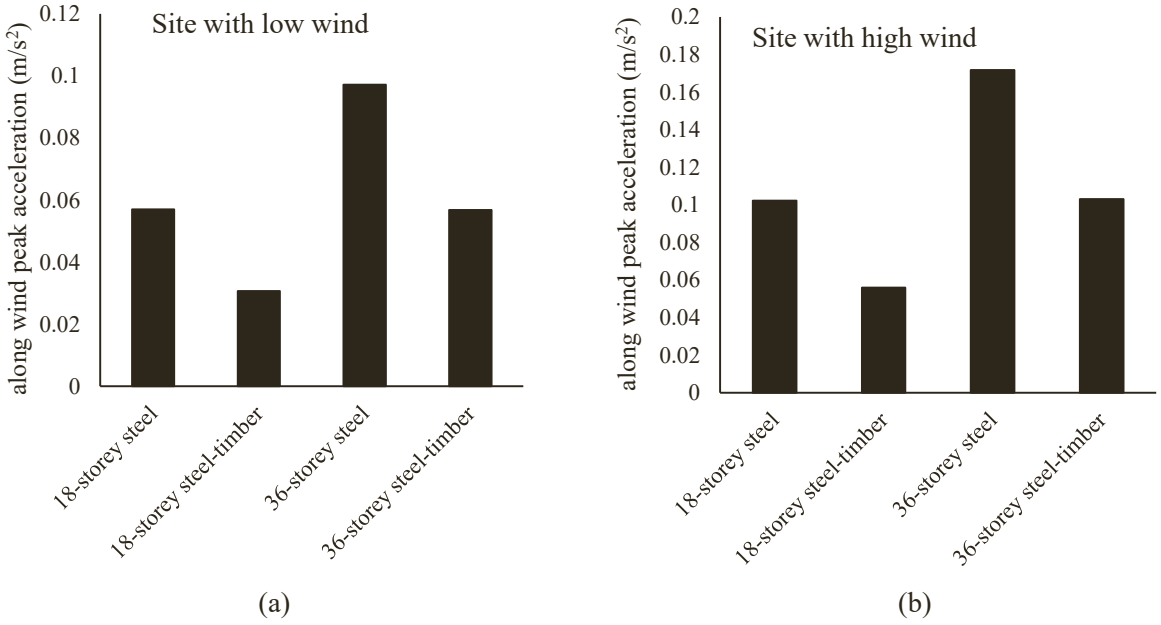

Fig. 11. Along-wind peak accelerations at the top floor of case study buildings: (a) site with low wind; (b) site with high wind.

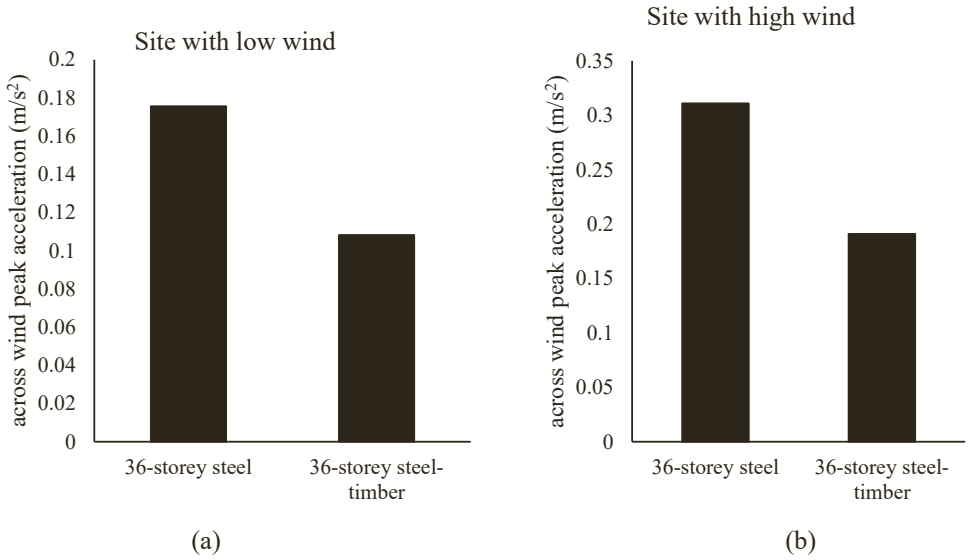

Fig. 12. Across-wind peak accelerations at the top floor of case study buildings: (a) site with low wind; (b) site with high wind.

captured by the simplified design procedure. Specifically, the relevance of higher modes is visible through an increase in drift from the 12th floor for 18-storeys structures (Fig. 14) while, for 36-storeys ones, the increase is more evident from the 24th floor onwards (Fig. 15). The target drift set during the DDBD design phase is achieved with good approximation for the 18-storey building, while it is (in average) exceeded in the upper floors of the 36-storey. .

Since one of the key peculiarities of the low-damage technology implemented in the steel-timber buildings is to bring back the structure to its original (before the seismic event) position, thanks to the re-centering action provided by the unbonded tendons/cable, it is important to analyze the response/performance also in terms of residual/permanent displacements/drifts. As shown in Fig. 16, the low-damage steel-timber buildings are subjected to significantly lower (averaged values of the residual interstorey drift obtained for each input signal) residual displacements when compared to those in steel buildings with traditional connections. However, even in the case of low-damage connections in the perimeter frames, the residual displacements are not nihil, due to the presence of BRB braces which, by plasticization, lead to permanent residual displacement/damage. A proper design procedure of such a peculiar dual system (BRB core plus steel-(Pres-lam) timber frames) should in fact adopt a higher moment-recentering ratio in the rocking-dissipating connections in order to account for the need to recover the permanent deformations/displacements/drifts generated by the BRBs braces.

Wind nonlinear dynamic analyses imply the numerical generation of artificial wind force time histories and their application to the FE model. In this work, the artificial time histories have been generated by an in-house developed MatLab® code by superimposing the mean and the turbulent contribution in each considered direction. Since they are well-established by the literature [27,28], for the sake of brevity, the equations implemented in the above-mentioned Matlab® code are not reported here. As a general description of the implemented models, it can be said that the turbulent components have been considered as

Table 4
DDBD key parameters for the four cases study building at the site with high-seismicity and low-wind: Target drift, target displacement, spectrum reduction factor, effective height, effective period, effective/secant stiffness, Base Shear.

Site with high seismicity - low wind				
	18-storyes Steel building	18-storeys Steel-timber building	36-storyes Steel building	36-storeys Steel-timber building
θ_d (%)	1.80	1.80	1.50	1.50
Δ_d (m)	0.77	0.77	0.92	0.92
η	0.72	0.80	0.76	0.80
H_{eff} (m)	43.02	43.05	84.75	84.71
H_{eff}/H_{tot} (%)	68.28	68.33	67.26	67.22
T_{eff} (s)	4.27	3.90	4.78	4.56
K_{eff} (kN/m)	10153.27	11806.36	30187.93	32599.63
M_{eff} (ton)	4689.46	4548.91	17472.20	17171.24
M_{eff}/M_{tot} (%)	76.88	76.87	104.90	104.91
V_b (kN)	3930.83	4574.43	14309.79	15400.43

Table 5
DDBD key parameters for the four cases study building at the site with high-seismicity and high-wind: Target drift, target displacement, spectrum reduction factor, effective height, effective period, effective/secant stiffness, Base Shear.

Site of low seismicity - high wind				
	18-storyes Steel building	18-storeys Steel-timber building	36-storyes Steel building	36-storeys Steel-timber building
θ_d (%)	1.00	1.00	0.80	0.80
Δ_d (m)	0.43	0.43	0.49	0.49
η	0.90	0.85	0.96	0.89
H_{eff} (m)	43.04	43.04	84.78	84.78
H_{eff}/H_{tot} (%)	68.32	68.32	67.29	67.29
T_{eff} (s)	4.72	5.01	5.08	5.44
K_{eff} (kN/m)	8294.19	7115.99	26585.56	22568.98
M_{eff} (ton)	4680.76	4524.48	17379.23	16918.66
M_{eff}/M_{tot} (%)	68.32	76.90	104.97	104.95
V_b (kN)	1784.94	1531.37	6751.85	5547.09

stationary zero-mean Gaussian ergodic stochastic processes. The turbulent components of the wind velocity (and consequently of the wind forces) in the along- and across- wind directions have been considered as uncorrelated each other; the torsional component of the wind has been neglected due to the regularity of the considered buildings. For each direction one wind velocity time history has been considered each floor of the building, then the wind force has been obtained from the wind velocity by taking into account the floor tributary area and the building aerodynamic coefficient. Turbulent velocities time series have been numerically generated by applying the Proper Orthogonal Decomposition (POD) technique to the power spectral density (PSD) matrices of the wind turbulent spectra in the two considered directions [29]. The Solari spectra [30] and the Liang et al. spectra [31] have been used for the definition of the PSD matrices in the along-wind and in the across-wind direction respectively for the description of the two turbulent spectra characteristics.

A total of 12 wind force time series for each direction (refereed as TH in the figures) have been identified for each case study.

The peak forces at each floor resulting from the numerically generated time series have been compared with the CNR-DT 207 R1/2018 equivalent static forces, determined as described in appendix of this paper. The comparison is shown in Fig. 17 for 18-floor building and 36-floor building in the across-wind direction and the high wind hazard construction site.

From Fig. 17, it can be argued that, while numerically generated time histories are the same for the two buildings typologies (they do not depend on the building dynamics), the equivalent static forces are related to the flexibility of the building and thus differ between steel and steel-timber buildings. Furthermore, for the 36 storey building, the equivalent static forces for steel-timber buildings are comparable with the average profile of the peaks of the numerically generated forces, while they are comparable with the average plus a standard deviation of the peak values for steel buildings. On the other side, the linear-like shape of the profile along the building's height is confirmed.

The peak values of the accelerations, at the top habitable floor level, have been evaluated, and these values have been then checked for the habitability through the perception thresholds described above.

The comparison of the top floor peak accelerations evaluated by the time history analyses at the high-wind hazard construction site, with the one obtained by the CNR method is shown in Fig. 18 for the 18-storey building and in Fig. 19 for the 36-storey building, together with the perception thresholds. Regarding the CNR peak accelerations, they have been evaluated by considering two different first modal frequencies for the structures: i) the one deriving from the preliminary estimation given by the CNR as reported in Eqs. (18) and (19) (indicated simply as "CNR" in the figure) and ii) the one obtained by the modal analysis (indicated as "CNR (Tmodal)" in the figure). The figures show that the peak accelerations evaluated with the CNR simplified method and the natural frequency estimated by Eqs. (18) and (19) are, on average, lower than those resulting from the application of time series ("average" in the figure), while the one evaluated by the CNR procedure but using the natural frequency obtained by the modal analysis, are higher than those resulting from the application of the time series, especially for the 36-storey steel building (Fig. 19-left). In all cases (average of the 12 TH values, "CNR" case and "CNT (Tmodal)" case), the comfort performance assessment is not satisfied, with the best case (18-storey steel-timber building in Fig. 18-right) falling exactly on the perception limit.

4. Integrated wind – earthquake performance-based design/assessment approach

4.1. ADRS domain for wind performance-based design

The Acceleration-Displacement Response Spectrumdomain, originally proposed as part of the Capacity Spectrum Method in the mid-1970 s, has been widely adopted in literature to study the response of a structure under earthquakes [32–34]. The Accelerations-Displacement Response Spectra (ADRS) curves are determined starting from the pseudo-acceleration elastic spectra according on the site, the nominal life and the class of the use of the building and the characteristics of the terrain roughness. Starting from these spectra that provide the values of the pseudo-accelerations (Sa), as a function of the building period (T), the pseudo-displacements (Sd), are obtained using Eq. (35):

$$S_d = \frac{S_a}{\frac{4\pi^2}{T^2}} g \tag{35}$$

For the wind, it is not usual to refer to the ADRS curves like for earthquake. But in this paper the ADRS format is shown to be an effective way to compare the two actions under a common language/nomenclatre, something that is crucial to obtain true MH design procedures [20].

Along-wind and across-wind accelerations are first obtained, with the simplified CNR procedure described in Section 2.2 and are then divided by the gravity to obtain pseudo accelerations. Such accelerations are determined for several cases: buildings with the same geometry and the same structural scheme but having different values of the bulk density ρ_m (varying between 20 e 400 kg/m^3) are considered. The fundamental natural frequency n_i of the building in the direction "i"

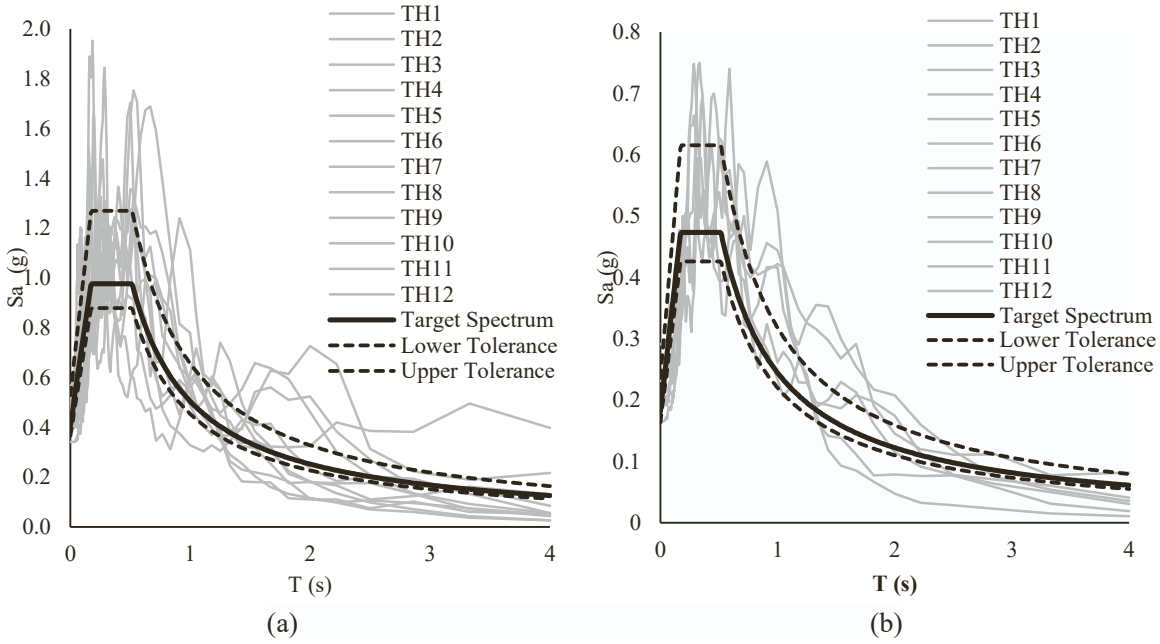

Fig. 13. Natural accelerograms: (a) high seismicity site; (b) low seismicity site (right).

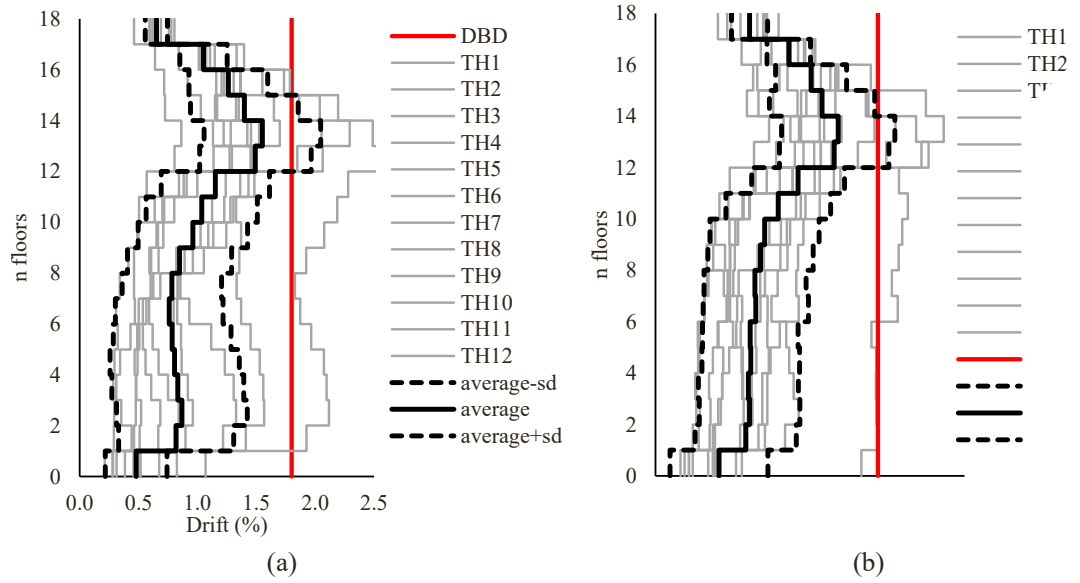

Fig. 14. Comparison between the maximum interstorey drifts obtained by the NLTHA and the DDBD target values for the site with high seismicity ☹ (a)18-storeys steel building; (b) 18-storeys Pres-Lam building.

(with i=D or L) dependents from ρ_m according to the Eq. (36).

$$n_i = \frac{1}{2\pi}\sqrt{\frac{K}{\rho_m \bullet V_{tot}}} \tag{36}$$

Where K is the stiffness of the case study building (evaluated as $K = (2 \bullet \pi)^2 \bullet \frac{m}{T}$), being "m" and "T" the modal mass and period of the considered mode, and V_{tot} is the total volume of the structure.

Given the pseudo accelerations, the Eq. (35), being valid for the base excitation case, cannot be applied in case of wind, then the displacements have been determined by applying the equivalent static forces (evaluated as reported in the appendix of the paper) to the FE structural models of the buildings. The variation of the bulk density for the evaluation of the wind ADRS has been imposed by assigning a multiplication factor to the masses deriving from the non-structural loads.

Depending on the bulk density value, the acceleration trend is determined by the previously described CNR procedure as a function of the oscillation frequency of the structure obtained by Eq. (36). High frequencies, low periods, high accelerations and high displacements correspond to low values of ρ_m.

The buildings are characterized by a double inertial symmetry in plan, then the first oscillation frequency is the same in the two orthogonal directions corresponding with the principal inertial axes of the floor, which also coincides with the along- and across- wind directions if it is assumed that the wind comes orthogonally to one of the building external vertical faces (most severe load conditions for across-wind building accelerations due to the occurring of the vortex shedding).

The trend of the peak top floor pseudo accelerations and pseudo

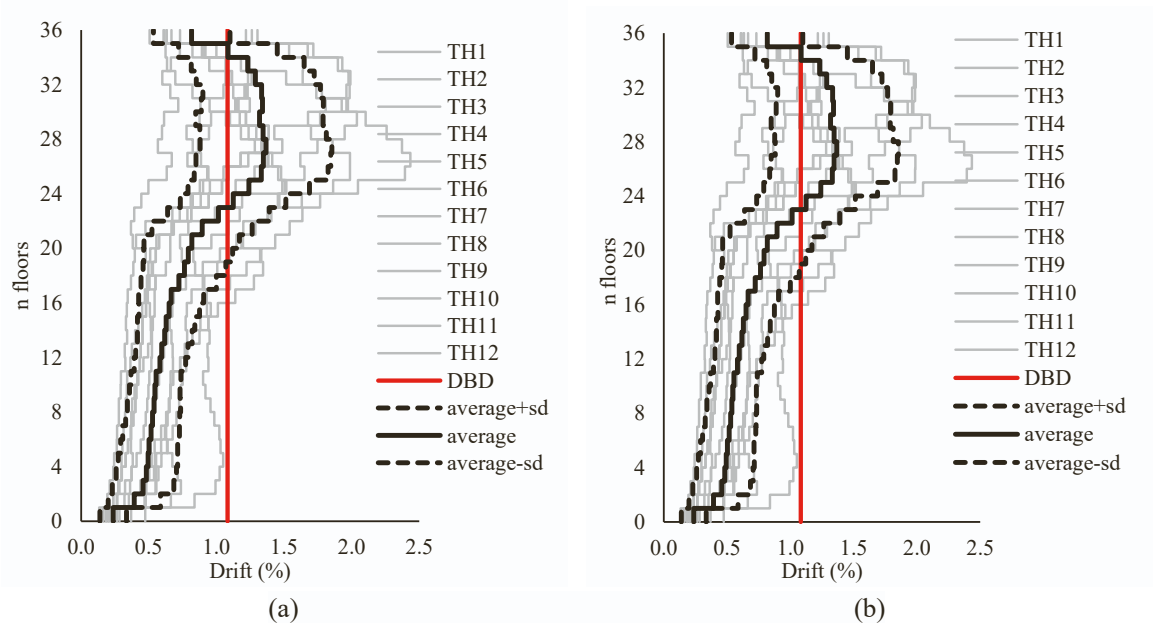

Fig. 15. Comparison between the maximum interstorey drifts obtained by the NLTHA and the DDBD target values for the site with high seismicity: (a) 36-storeys steel building; (b) 36-storeys Pres-Lam building.

Table 6
Natural seismic signals for low seismicity-high wind site.

	ID Code	ID Station	Date	Epicentral distance (km)	PGA (m/s^2)	PGV (m/s)	Mw
TH1	IT-2012-0011	SAN0	29/05/2012	15.8	2.167	0.351	6.0
TH2	EMSC-20181226_0000014	EVRN	26/12/2018	5.3	2.948	0.278	4.9
TH3	IT-2012-0011	SAN0	29/05/2012	6.1	1.709	0.195	6.0
TH4	EMSC-20160824_0000006	NOR	24/08/2016	15.6	1.767	0.211	6.0
TH5	IT-2012-0011	T0811	29/05/2012	14.3	2.020	0.239	6.0
TH6	IT-1997-0006	CSA	26/09/1997	22.3	1.688	0.134	6.0
TH7	IT-2012-0010	T0819	29/05/2012	6.8	2.531	0.428	5.5
TH8	EMSC-20161026_0000077	NOR	26/10/2016	9.5	1.632	0.160	5.4
TH9	IT-1997-0006	CLF	26/09/1997	4.8	2.234	0.171	6.0
TH10	EMSC-20161026_0000095	NOR	26/10/2016	13.3	2.108	0.210	5.9
TH11	IT-2012-0011	T0802	29/05/2012	9.9	2.908	0242	6.0
TH12	IT-2009-0009	AQK	06/04/2009	1.8	3.555	0.358	6.1

Table 7
Natural seismic signals for high seismicity-low wind site.

	ID Code	ID Station	Date	Epicentral distance (km)	PGA (m/s^2)	PGV (m/s)	Mw
TH1	EMSC-20161030_0000029	T1201	30/10/2016	22.6	4.737	0.830	6.5
TH2	EMSC-20161030_0000029	MZ102	30/10/2016	17.4	3.972	0.481	6.5
TH3	EMSC-20161030_0000029	ACC	30/10/2016	18.6	5.469	0.441	6.5
TH4	EMSC-20161030_0000029	MZ04	30/10/2016	23.1	7.933	0.854	6.5
TH5	IT-2009-0009	AQV	06/04/2009	4.9	6.442	0.427	6.1
TH6	EMSC-20161026_0000077	CMI	26/10/2016	3.7	7.068	0.557	5.4
TH7	EMSC-20161030_0000029	CNE	30/10/2016	7.7	5.365	0.382	6.5
TH8	IT-2012-0011	MRN	29/05/2012	4.1	8.407	0.575	6.0
TH9	IT-1984-0002	NCR	29/04/1984	20.6	2.008	0.059	5.6
TH10	EMSC-20161030_0000029	FCC	30/10/2016	11.0	9.311	0.773	6.5
TH11	EMSC-20181226_0000014	SVN	26/12/2018	4.5	5.479	0.371	4.9
TH12	IT-2010-0032	ILLI	16/08/2010	11.4	3.822	0.221	4.7

displacements with the building vibration period T are shown in Fig. 20 e Fig. 21 for the along and across wind directions respectively, and by considering pre-definite values of the wind speed intensity corresponding to the specified return periods TR taken equal to 1, 10 or 100 years at the construction site with high-wind hazard.

It can be seen in the figures both in along- and across- wind directions that, while the peak top floor displacements trend is always increasing with T, the peak top floor accelerations are initially increasing and then decreasing with the period T.

The trends shown in Fig. 20 e Fig. 21 can be used to obtain the ADRS curves for wind simply by considering the values of pseudo displacements and pseudo accelerations at different "T" values. The ADRS curves allow to compare the actions deriving from the earthquake and the wind hazards at different intensity levels. The ADRS curves are derived for all the LSs introduced above: the SLS, which corresponds to the damage limit state for a return period TR of 101 years of the earthquake and to

Table 8
Dominant action for each case study according to the minimum addedd stiffness.

	18-storyes Steel building	18-storeys Steel-timber	36-storyes Steel	36-storeys Steel-timber
Site with high seismicity and low wind	+ 15.6% Earthquake dominates	+ 48.4% Earthquake dominates	+ 40.4% Wind dominates	+ 27.0% Wind dominates
Site with low seismicity and high wind	+ 36.1% Wind dominates	+ 5.8% Wind dominates	+ 67.7% Wind dominates	+ 64.6% Wind dominates

the occupants' comfort limit state for a TR of 10 years for the wind, and the ULS, that corresponds to the life safety for the earthquake (949 years of TR) and to linear elastic operational condition (TR of 100 years) for the wind.

The ADRS curves obtained for the considered TR, have the shape shown in Fig. 22 (36-storey steel-wood building at the construction site with low seismicity and high wind), where it is possible to understand which of the two hazards is dominant, according to the oscillation period of the structure both for SLS and ULS. For example, from the left-side pane of Fig. 22 it is clear that for periods $T > 1$ s, across-wind hazard is dominant at SLS, while it can be argued from the right-side panel that at ULSs the earthquake is dominant for periods $T < 2$ s, while the along-wind become dominant for periods $T > 2$ s .

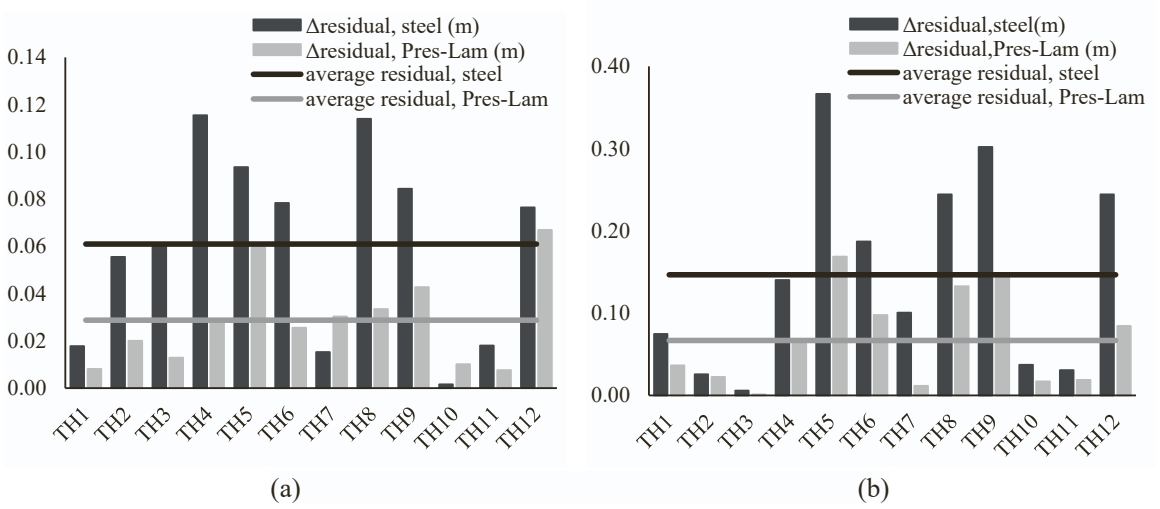

Fig. 16. Comparison between the residual displacements [m] of buildings with hybrid connections (grey) and those of buildings with traditional connections (black): (a) 18-storeys; 36-storeys building on the right.

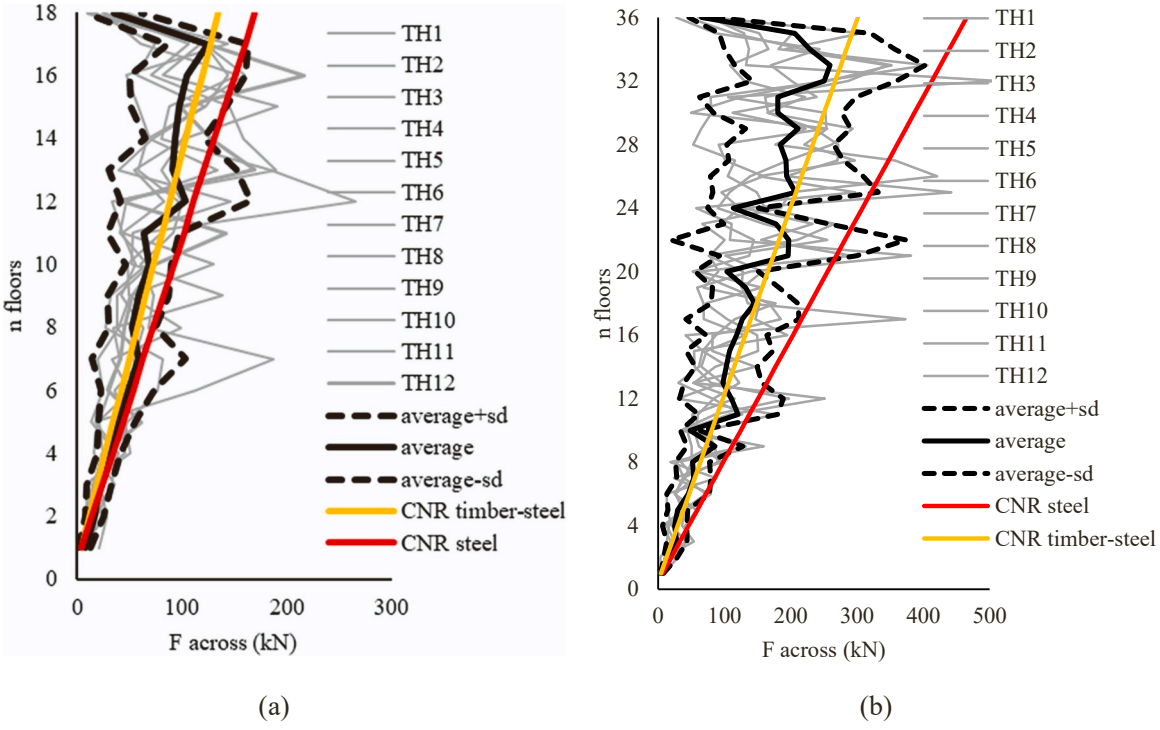

Fig. 17. Comparison between the peak values of the artificial wind force time series at different floors and the equivalent static forces for the site with high wind hazard): (a) 18-storeys; 36-storeys building on the right.

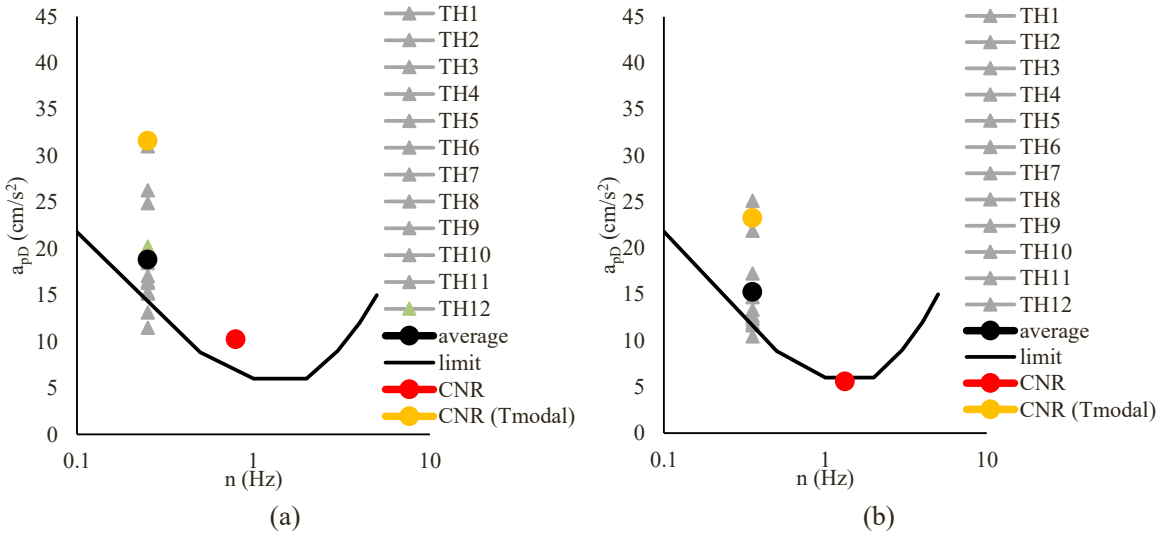

Fig. 18. Comparison between the peak longitudinal accelerations: (a) 18-storeys structures with traditional connections; (b) 18-storeys structures with hybrid connections.

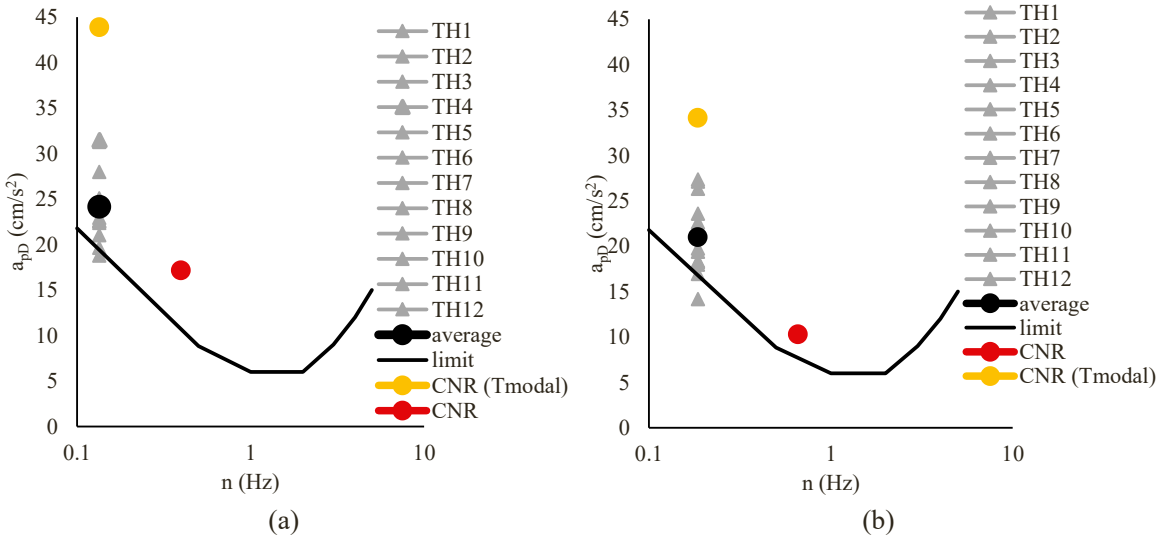

Fig. 19. Comparison between the peak longitudinal accelerations: (a) 36-storeys structures with traditional connections; (b) 36-storeys structures with hybrid connections.

4.2. Multi-Hazard ADRS domain comparisons

The above-mentioned comparison in terms of ADRS curves has been made for all the considered cases. The figures below show the case-by-case comparisons made for the construction site with low seismicity-high wind grouped by considered Limit States and by the building heights.

From the figures above, it is possible to notice how, in the buildings of 18 floors, the earthquake would always governs the design: both at serviceability conditions and at the ultimate limit state. The relevance of the wind increases with the increase in the building height, in fact, for the 36-storeys structures, the ADRS curves, relative to the wind, are greater than those of the earthquake at the SLS for both typologies. Wind is also dominant at ULSs for the 36-storey steel building in steel, while the two hazards are comparable for the engineered wood and steel building at ULSs. In fact, as expected, the increasing of the importance of the wind hazard is more visible in cases where the structures are more flexible and therefore in those made entirely of steel and without hybrid connections. However, the 36 floors building at the SLS the action of the wind always governs on the earthquake.

Finally, a comparison has been made to determine, on a case-by-case basis, what is the dominant/governing design action. Starting from the initial buildings' design configuration analyzed in Section 3.5, which is not verified for either earthquake or wind loading, the minimum stiffness/strength mass addition to the buildings (obtained by increasing the cross-sections and then determining the natural frequency) letting the performances reaching the required level as established in the design phase has been evaluated. This has been done for earthquake by estimating the stresses to which all the elements were subjected, the minimum sections necessary to withstand these stresses and, consequently, the minimum area of braces, columns and beams have been determined. For the wind, this has been done by checking that the peak acceleration of the top floor was below the threshold of perception. The necessary minimum added stiffness, expressed as a percentage, are given for each case study, is shown in Table 3. The dominant design action between earthquake and wind (also indicated in the table), is identified as the one requiring the larger added mass (as specified above).

From the table, it can be sees how, only in the cases of 18-storeys

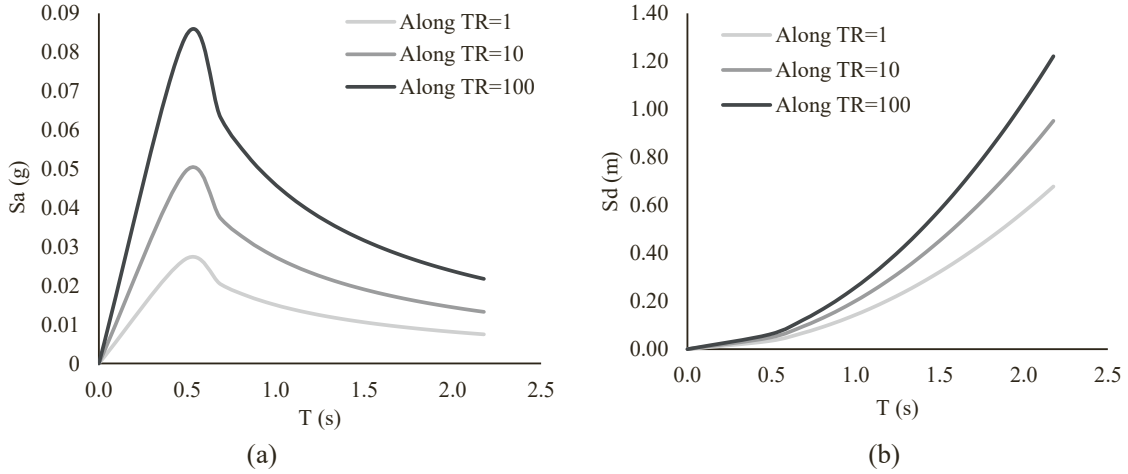

Fig. 20. Along-wind direction: (a) trend of the peak top floor accelerations with the building vibration period; (b) trend of the peak top floor displacements with the building vibration period.

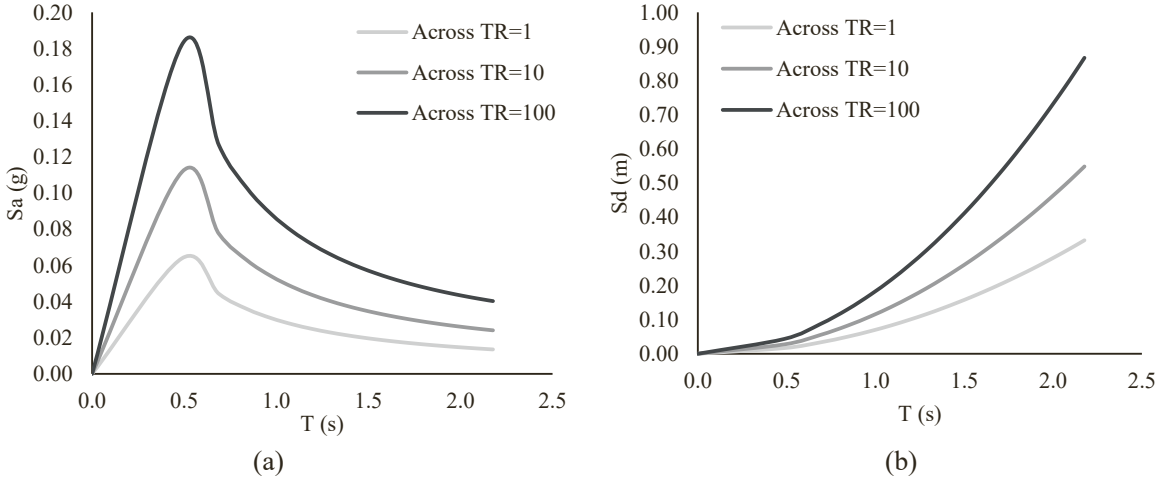

Fig. 21. Across-wind direction: (a) trend of the peak top floor accelerations with the building vibration period;(b) trend of the peak top floor displacements with the building vibration period.

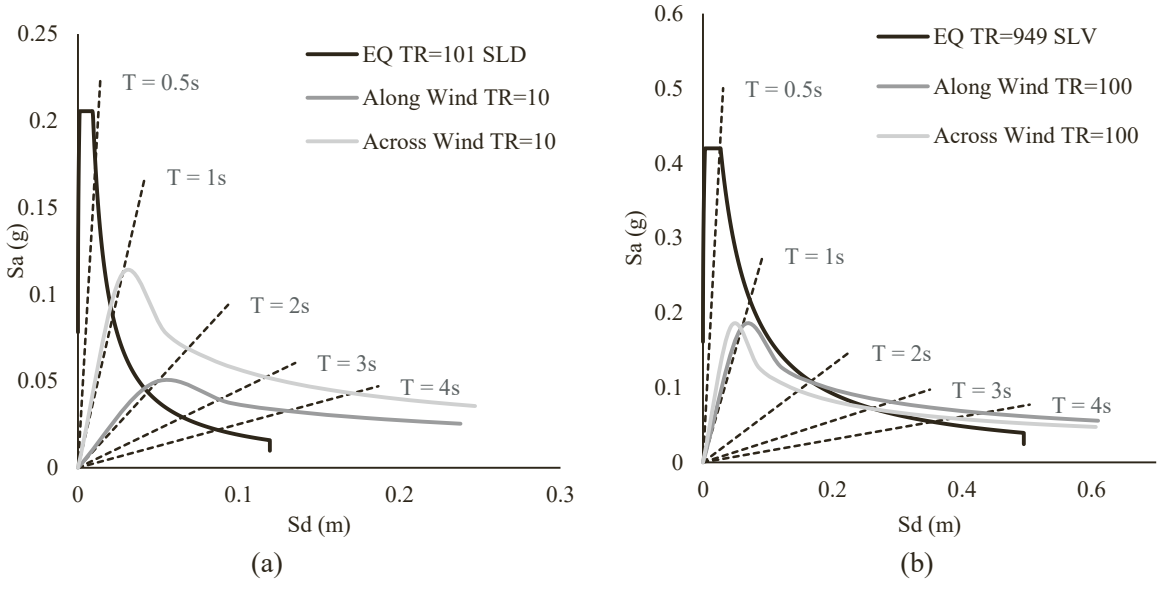

Fig. 22. Example of Earthquake – Wind comparison in terms of ADRS curves at the site with low seismicity-high wind: (a) SLS; (b) ULS.

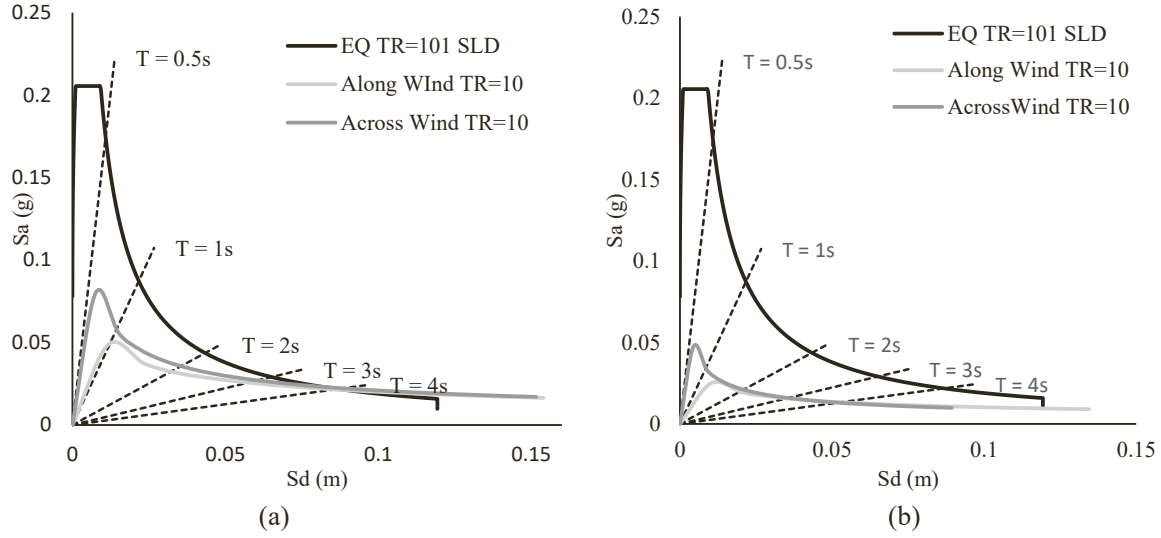

Fig. 23. Earthquake – Wind comparison in terms of ADRS curves for the SLS at the site with low seismicity-high wind: (a) 18-storeys steel buildings; (b) 18-storeys engineered wood and steel buildings.

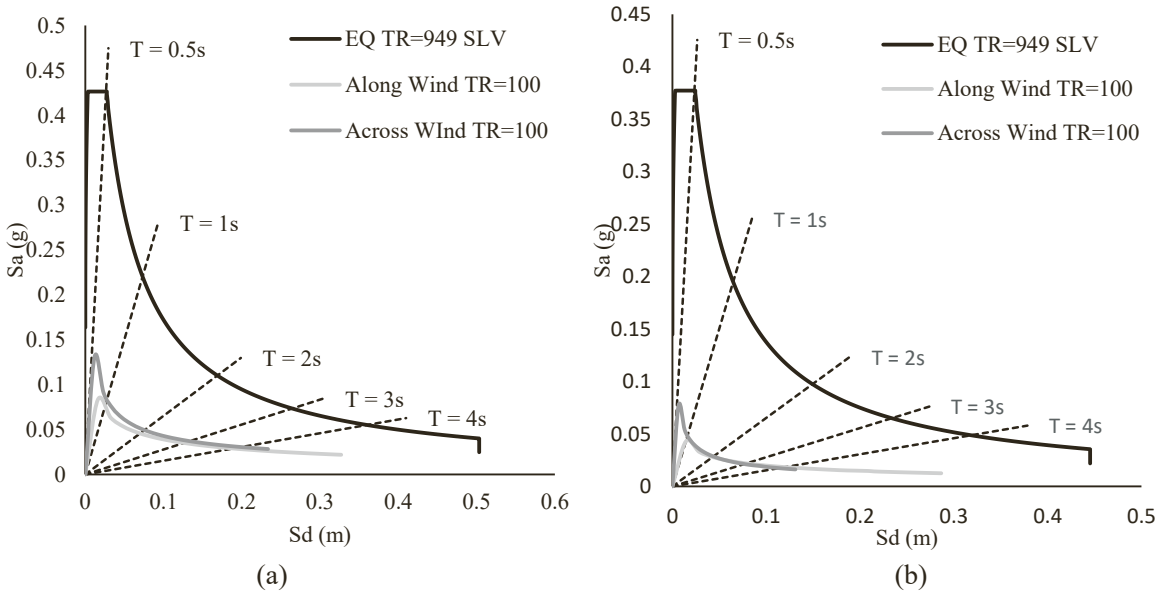

Fig. 24. Earthquake – Wind comparison in terms of ADRS curves for the SLS at the site with low seismicity-high wind: (a) 18-storeys steel buildings; (b) 18-storeys engineered wood and steel buildings (right) at the ULS. Site with low seismicity-high wind.

steel and steel-timber buildings located in the high-seismicity low-wind construction site, the earthquake is dominant, while in all other cases the wind dominates. The latter becomes increasingly important as the number of floors of the building increases. Finally, it can be observed how the minimum required added mass is larger for steel buildings than for engineered wood and steel structures with hybrid connections.

4.3. Multi-Hazard preliminary design methodology

As discussed in Sections 2 and 3.2, the preliminary design of the buildings has been conducted by taking into account the two hazards individually. On the other hand, as already said in the introduction, in a true multi-hazard view, the preliminary design phase should be conducted by considering simultaneously earthquake and wind. With this in mind, a methodology is proposed in this section to allow the multi-hazard preliminary design by using the ADRS comparison method introduced in previous parts. Two limit values have been superimposed on the ADRS plane: the first is referred to the wind induced SLSs by checking the peak accelerations of the top floor, with a return period TR= 10 years; the second limit value is given by a drift limit linked to the ULS under earthquake. The first value provides the initial stiffness that the structure should have so that the verification of habitability is respected, the second, instead, defines the target demand for ductility of the system. Thus, an ideal capacity curve has been obtained.

The case of the building of 36 floors made of steel and timber with hybrid connections and placed in the area of low seismicity and high wind is shown in Fig. 27. Only the transverse component of the wind is represented because it is the most significant.

By having this ideal capacity curve in the preliminary design phase, the target elastic stiffness and ductility are then defined by taking into account both wind and earthquake hazards.

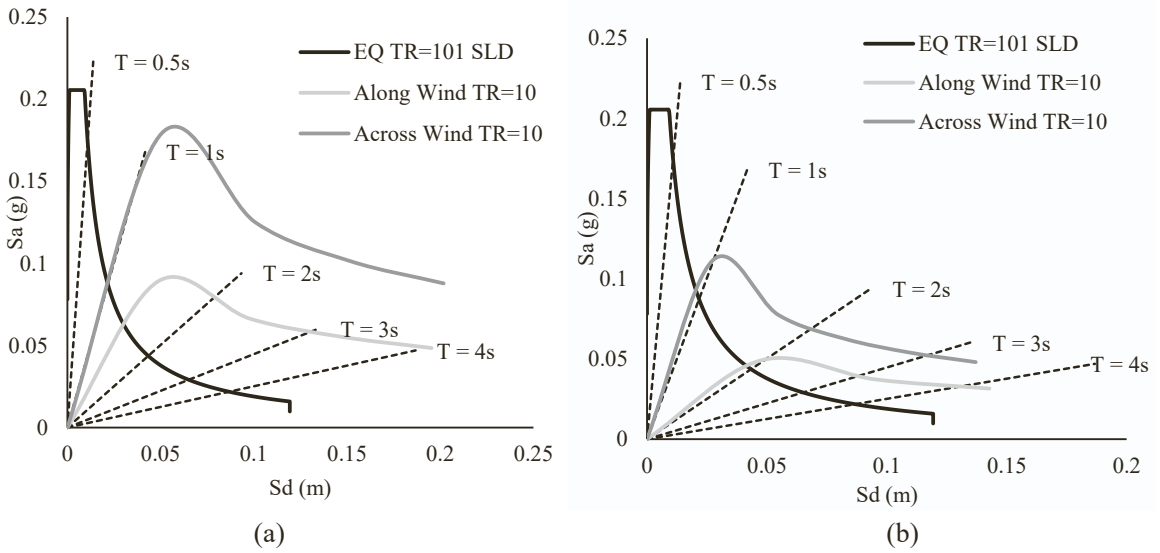

Fig. 25. Earthquake – Wind comparison in terms of ADRS curves for the SLS at the site with low seismicity-high wind: (a) 36-storeys steel buildings; (b) 36-storeys engineered wood and steel buildings.

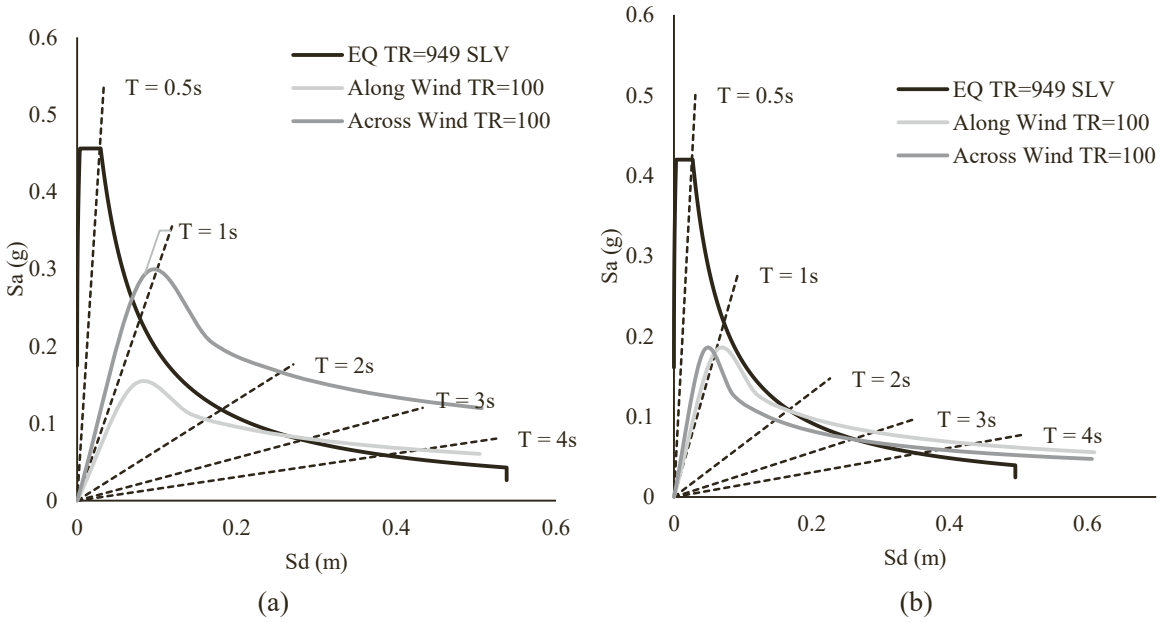

Fig. 26. Earthquake – Wind comparison in terms of ADRS curves for the ULS at the site with low seismicity-high wind; (a) 36-storeys steel buildings; (b) 36-storeys engineered wood and steel buildings.

5. Conclusions

The aim of the work was to study the behavior of tall buildings with structural elements in engineered wood and low damage connections, subjected to horizontal wind and earthquake actions and compare them with structures characterized by the same geometric characteristics but made in steel with traditional bolted connections. An innovative comparison method based on an integrated/jointed ADRS qind-earthquake capacity-demand performance representation is proposed in the paper. Then the same representation is used to present a Multi-Hazard (MH) preliminary design approach which allows to define the target elastic stiffness, strength and ductility for the building.

First, some case study buildings of different heights located in different construction sites (i.e., characterized by low or high intensity for the two hazards in turn) are preliminarily designed under vertical and seismic loads, then the performances of the buildings under wind and earthquake are assessed by a detailed analysis. The peak interstorey drift has been chosen as response indicator for ULSs under wind and earthquake, while SLSs have been checked by comparing the peak floor accelerations with the motion perception thresholds indicated by the Guidelines. The detailed comparison between the performances of the two analyzed building typologies (steel with bolted connections or steel-timber with low damage connections) under wind and earthquake has been conducted by Non-Linear Time History Analyses (NLTHA) with the avail of natural seismic signals (recorded ground motions) and artificially generated time series for the floor wind forces. This type of analysis has confirmed the ability of hybrid connections to minimize structural damage (both in terms of maximum and residual displacement/drift). In particular, it has been seen that buildings with traditional connections were subjected to more significant residual/

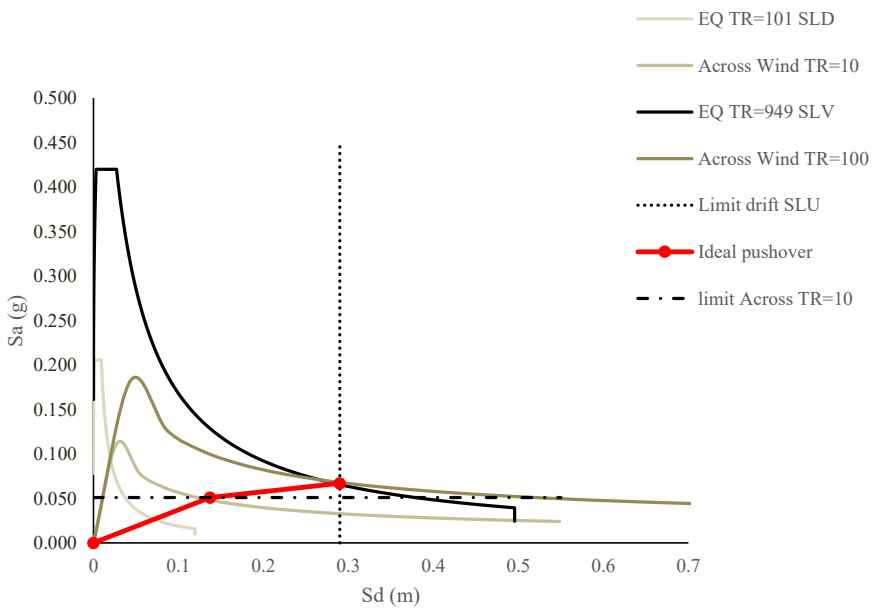

Fig. 27. Ideal curve for steel - timber building of 36 floors, placed in the construction site of low seismicity and high wind.

permanent displacements. Regarding the performances under wind, in most cases, accelerations were not below the perception thresholds, especially in buildings without hybrid connections.

Finally, in a MH view, the actions of wind and earthquake have been compared in terms of structural masses and in terms of ADRS curves. The results showed that, as expected, the action of the wind becomes more and more important as the number of floors increases while, for the structures with hybrid connections, the preponderance of the wind on the earthquake attenuates. The comparison in terms of ADRS curves allowed to identify capacity an ideal curve for the building by introducing 2 limit values for the response parameters, each corresponding to a limit state. Specifically, the first is related to accelerations induced by wind and provides the initial stiffness that the structure must have in order to ensure comfort for the occupants, while the second is a drift limit associated to the ultimate limit state and affects the ductility demand and, in turns, the actual energy dissipation. The ideal capacity curve can be used to preliminary design the building in a true MH approach by considering both wind and earthquake.

CRediT authorship contribution statement

Ciabattoni Micol: Formal analysis, Software, Writing – original draft. **Petrini Francesco:** Conceptualization, Funding acquisition, Methodology, Writing – review & editing. **Pampanin Stefano:** Conceptualization, Funding acquisition, Methodology, Writing – review & editing.

Declaration of Competing Interest

The authors declare that they have no known competing financial interests or personal relationships that could have appeared to influence the work reported in this paper. Francesco Petrini reports was provided by University of Rome La Sapienza.

Data availability

Data will be made available on request.

Aknowledgments

The Financial support of the Research Project No. CN1221844D08208F from Sapienza University of Rome under the umbrella of the national program PNRR – CN1 – Spoke 5 (Directorial Decretation no. 1031 of June, 17th, 2022) is gratefully acknowledged.

APPENDIX A. Equivalent static wind actions for displacement response evaluation

As well known, the analysis of the wind actions and their effects on the structures is based on the assessment of the wind speed at the construction site. The wind speed consists of two components: an average part that varies slowly over time and space and a turbulent fluctuation with zero average that varies rapidly over time and space. The values of two components depend on the geographical position, the altitude above sea level of the construction site, the roughness and topography of the terrain and the considered return period.

Then the wind exerts a set of aerodynamic forces on the construction and its elements in accordance with the shape, orientation and the extension of the structure. These aerodynamic actions are schematized by a longitudinal (along-wind) force f_D (D = Drag), a lateral (across-wind) force f_L (L = Lift) and a torsional moment m_M. Following these actions, the structure exhibit the response in three directions: longitudinal, lateral and torsional, as shown in Figure A1.

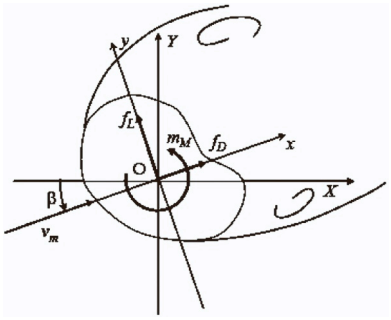

Figure. A1. Two-dimensional body in a wind field (after CNR 2018).

.

For buildings with a regular shape and ordinary dimensions, the displacements induced by the wind can be assessed through equivalent forces that are estimated to derive, when statically applied to the construction, the maximum effects induced by the dynamic application of the actual wind dynamic actions. The equivalent static actions are the product of the peak aerodynamic stationary actions and the dynamic amplification coefficients. The latter depend on the dynamic parameters of the structure, the characteristics of the incident wind, the geometry and the dimension of the construction (the last one influencing the spatial correlation of the turbulent wind force components). The lateral actions increase in importance with the height, slenderness and flexiblity of the building, while the torsional action can be neglected in the preliminary design phase if the structure is regular in plan and elevation. The procedure for evaluating equivalent static actions is summarized with a flowchart in Figure A2. Equivalent static actions can be used to be applied to a FE model to evaluate the peak displacements experimented by the building under the design wind.

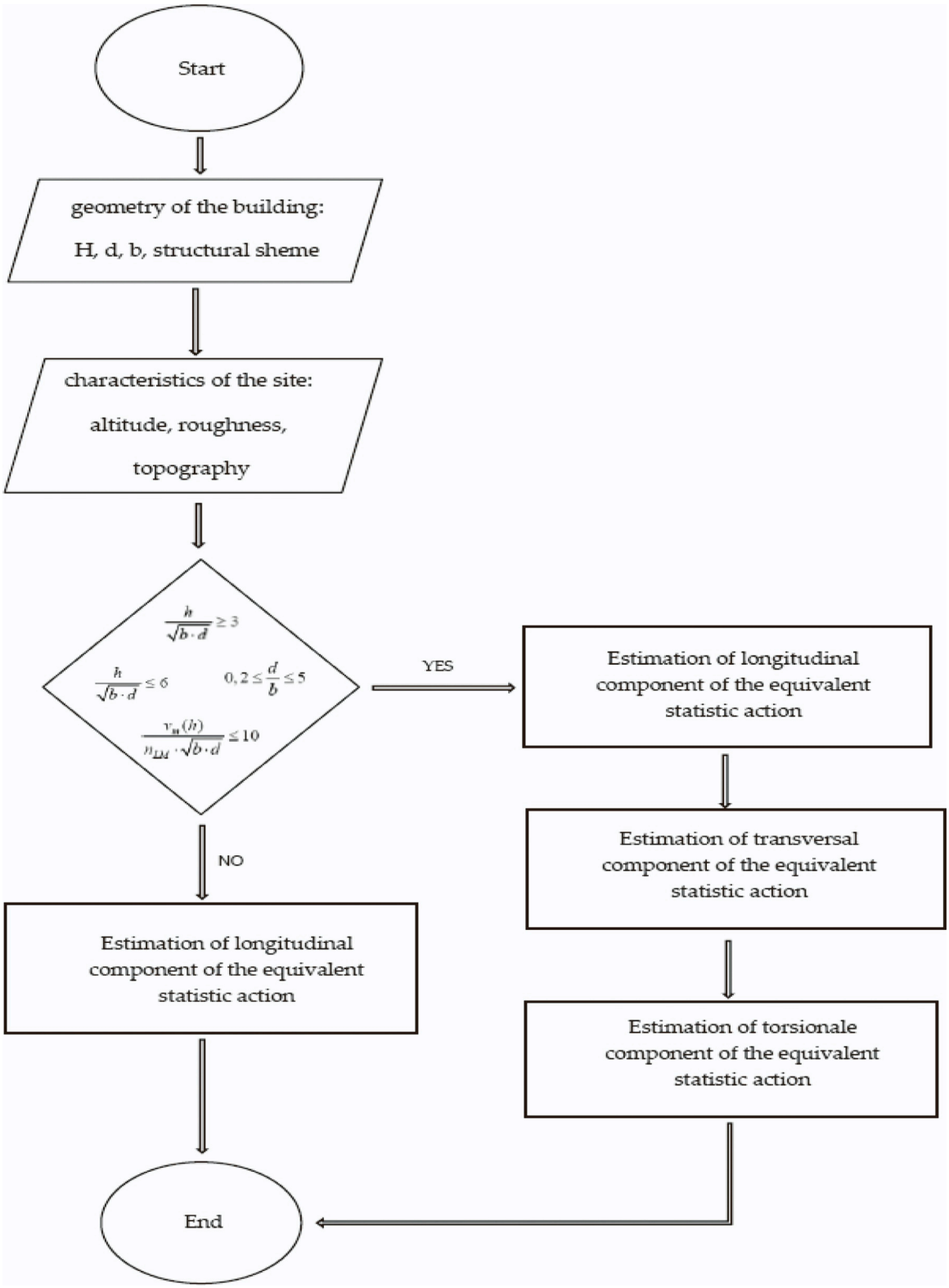

Fig. A2. Procedure used for evaluating equivalent static wind forces.

.

In order to evaluate displacements under wind, in this paper the actions of the wind are represented by equivalent load distributions which, applied statically, generate the maximum values of the stresses induced by the actual action of the wind. In particular, the actions and effects induced by the wind in the along-wind, across-wind and twisting directions have been evaluated. For this purpose, it has been necessary to define the characteristics of the incident wind, according to the selected sites for the buildings, thus, to determine the reference speed, fundamental for the assessment of the displacement response.

The three following equations refer respectively to the along-wind, across-wind and torsional equivalent static actions:

$$F_D = (c'_{pe} q'_p + c''_{pe} q''_p) \bullet b \bullet \Delta \bullet c_{dD} \tag{A.1}$$

$$f_L(z) = 3 \bullet q_p(h) \bullet C_L \bullet b \bullet \frac{z}{h} \bullet c_{dL} \tag{A.2}$$

$$m_M(z) = 1.8 \bullet q_p(h) \bullet C_M \bullet b^2 \bullet \frac{z}{h} \bullet c_{dM} \tag{A.3}$$

Where:

c'_{pe} and c''_{pe} are the external pressure coefficients for the windward wall and the leeward face respectively:

$$c'_{pe} = 0.8 \tag{A.4}$$

$$c''_{pe} = -0.5 - 0.05 \bullet (h/d - 1) \tag{A.6}$$

q'_p and q''_p are the peak kinetic pressures for the windward wall and the leeward face respectively:

$$q'_p = \frac{1}{2} \bullet \rho \bullet v_r^2 \bullet c'_e(z) \tag{A.7}$$

$$q''_p = \frac{1}{2} \bullet \rho \bullet v_r^2 \bullet c''_e(z) \tag{A.8}$$

c'_e and c''_e are the exposure coefficients:

$$c'_e(z) = k_r^2 \bullet \ln(\frac{z}{z_0}) \bullet c_t(z) \bullet [\ln(\frac{z}{z_0}) \bullet c_t(z) + 7] \tag{A.9}$$

$$c''_e(z) = k_r^2 \bullet \ln(\frac{z_{\min}}{z_0}) \bullet c_t(z_{\min}) \bullet [\ln(\frac{z_{\min}}{z_0}) \bullet c_t(z_{\min}) + 7] \tag{A.10}$$

K_r, z_0 e z_{min} are respectively the soil factor, the roughness length and the minimum height whose values are provided by the CNR-DT 207 R1/2018 as a function of the exposure category.

C_t is the topographic coefficient whose value is provided by the CNR according to the orographic and topographic characteristics of the site.

V_r is the design reference speed and it is the value of the average wind speed over an interval time of 10 min, at a height of 10 m above the ground, on a flat and homogeneous ground with roughness length of 0.05 m, referred to the design period return.

Δ is the height of the segments in which the building is divided along its height to consider the non-uniform distribution of the equivalent static forces.

c_{dD} is the longitudinal dynamic coefficient:

$$c_{dD} = \frac{G_D}{1 + 7 \bullet I_v(z_e)} \tag{A.11}$$

$$G_D = 1 + 2 \bullet g_D \bullet I_v(z_e) \bullet \sqrt{B_D^2 + R_D^2} \tag{A.12}$$

$$I_v = \frac{1}{\ln(\frac{z}{z_0}) \bullet c_t} \tag{A.13}$$

$$g_D = \sqrt{2 \bullet \ln(\nu_D \bullet T)} + \frac{0.5772}{\sqrt{2 \bullet \ln(\nu_D \bullet T)}} \tag{A.14}$$

$$\nu_D = n_D \bullet \sqrt{\frac{R_D^2}{B_D^2 + R_D^2}} \tag{A.15}$$

$$B_D^2 = \frac{1}{1 + 0.9 \bullet (\frac{b+h}{L_v(z_e)})^{0.63}} \tag{A.16}$$

$$L_v(z_e) = \underline{L} \bullet (\frac{z}{\hat{z}})^k \tag{A.17}$$

$\hat{z}$ is equal to 200, $\underline{L}$ is equal to 300 and k is a coefficient according to exposure category of the site.

$$R_D^2 = \frac{\pi}{4 \bullet \xi_D} S_D \bullet R_h \bullet R_b \tag{A.18}$$

$$S_D = \frac{6.868 \bullet n_D \bullet \quad L_v(z_e)/\quad v_m(z_e)}{[1 + 10.302 \bullet n_D \bullet \quad L_v(z_e)/\quad v_m(z_e)]^{5/3}} \tag{A.19}$$

$$R_b = \begin{cases} 1per & n_b = 0 \\ \frac{1}{n_b} - \frac{1}{2 - n_b^2}(1 - e^{-2 \bullet n_b})per & n_b > 0 \end{cases} \tag{A.20}$$

$$R_h = \begin{cases} 1per & n_h = 0 \\ \frac{1}{n_h} - \frac{1}{2 - n_h^2}(1 - e^{-2 \bullet n_h})per & n_h > 0 \end{cases} \tag{A.21}$$

$$n_b = 4 \bullet \frac{n_D \bullet b}{v_m(z_e)} \tag{A.22}$$

$$n_h = 4 \bullet \frac{n_D \bullet h}{v_m(z_e)} \tag{A.23}$$

For the calculation of the aerodynamic coefficients c_{dL} and c_{dM} the procedure is similar to the one just described.

References

[1] Palermo A, Pampanin S, Calvi GM. Concept and development of hybrid solutionsfor seismic resistant bridge systems. J Earthq Eng 2005;9(6):899–921.
[2] Priestley MJN, Sritharan S, Conley JR, Pampanin S. Preliminary results and conclusions from the PRESSS five-story precast concrete test building. PCI J 1999; 44(6):42–67.
[3] NZCS (2010). PRESSS Deign Handbook, (Editor: S. Pampanin), New Zealand Concrete Society, Wellington, March.
[4] Sarti F., Smith T., Palermo A., Pampanin S., Carradine D.M. (2013). Experimental and analytical study of replaceable Buckling-Restrained Fuse-type (BRF) mild steel dissipaters. Conference of the New Zealand Society for Earthquake Engineering (2013 NZSEE Conference), Wellington, 26–28 April 2013. Available at http://db.nzsee.org.nz/2013/Paper_29.pdf (accessed on April, 08, 2021).
[5] Pampanin, S., Christopoulos, C. and Priestley M.J.N., (2002). Residual Deformations in the Performance-Based Seismic Assessment of Frame Systems, Research Report ROSE (European School on Advanced Studies on Reduction of Seismic Risk) 2002/2, Pavia, pp. 226.
[6] Marriott D, Pampanin S, Bull D, Palermo A. Dynamic testing of precast, post-tensioned rocking wall systems with alternative dissipating solutions. Bull NZ Soc Earthq Eng 2008;41(2):90–103.
[7] fib (2003), Seismic Design of Precast Concrete Building Structures. International Federation for Structural Concrete (fib), Bulletin No. 27, Lausanne, Switzerland, 254 pp.
[8] Miliziano A, Granello G, Palermo A, Pampanin S. Overview of connection detailing for post-tensioned dissipative timber frames. Struct Eng Int 2020;30(2):209–16. https://doi.org/10.1080/10168664.2020.1736968.
[9] Priestley M.J.N., Calvi G.M., Kowalsky M. Displacement-Based Seismic Design of Structures (2nd Edition). IUSS Press, Pavia, Italy, 2007.
[10] Boggs D., Dragovich J. (2006). The Nature of Wind Loads and Dynamic Response. CPP online report SP-240—2. Available at ⟨https://www.cppwind.com/wp-content/uploads/2020/12/WindLoadsDynamicResponses-Boggs2006.pdf⟩ (accessed April, 9, 2021).
[11] ISO 10137: Bases for design of structures – Serviceability of buildings and walkways against vibrations, International Standards Organization, 2007.
[12] CNR- National Research Council of Italy, Guide for the assessment of wind actions and effects on structures CNR-DT 207 2008, Rome, June 2010. Available at: ww.cnr.it/en/node/2642 (accessed Sept, 9, 2023).
[13] Petrini, F., Gkoumas, K., Rossi, C. Bontempi, F. (2020). Multi-Hazard Assessment of Bridges in Case of Hazard Chain: State of Play and Application to Vehicle-Pier Collision Followed by Fire. Frontiers in Built Environment - Bridge Engineering, 15 September 2020.
[14] Argyroudis SA, Mitoulis SA, Hofer L, Zanini MA, Tubaldi E, Frangopol DM. Resilience assessment framework for critical infrastructure in a multi-hazard environment: case study on transport assets. Sci Total Environ 2020;714:136854.
[15] Maley TJ, Sullivan TJ, Della Corte G. Development of a displacement-based design method for steel dual systems with buckling-restrained braces and moment-resisting frames. J Earthq Eng 2010;14(S1):106–40.
[16] Ponzo F.C., Di Cesare A., Lamarucciola N., Nigro D. (2019). Seismic Design and Testing of Post-tensioned Timber Buildings With Dissipative Bracing Systems. Frontiers in Built Environment -Earthquake Engineering, 06 September 2019.
[17] Sullivan T.J., Priestley M.J.N., Calvi G.M. (eds). A Model Code for the Displacement-Based Seismic Design of Structures DBD1, IUSS press, Pavia, Italy, 2012.
[18] Pampanin S., Marriott D., Palermo A. PRESSS Design Handbook. NZ Concrete Society Inc., Auckland, New Zealand, 2010.
[19] ASCE (2019), Prestandard for Performance-Based Wind Design, American Society of Civil Engineers, Reston, VA, USA.
[20] Petrini F, Francioli M. Next generation PBWE: extension of the SAC-FEMA method to high-rise buildings under wind hazards. Struct Saf 2022;99:102255. https://doi.org/10.1016/j.strusafe.2022.102255.
[21] Francioli M, Petrini F, Bontempi F. Structural robustness analysis of RC frames under seismic and blast chained loads scenarios. J Build Eng 2023;Volume 67: 105970. https://doi.org/10.1016/j.jobe.2023.105970.
[22] Watanabe, A., Hitomoi, Y., Saeki, E., Wada, A. and Fujimoto, M. (1988). Properties of braced encased in buckling-restraining concrete and steel tube. Proceedings of the 9th World Conference on Earthquake Engineering, Tokyo-Kyoto, Japan, Vol.IV, 719–724.
[23] CSI (Computers & Structures Inc) (2016). SAP2000 CSI Analysis Reference Manual, version 19.
[24] Chou CC, Chen SY. Subassemblage tests and finite analyses of sandwiched buckling-restrained braces. Eng Struct 2010;32. 2108-21 21.
[25] Tsai K.C., LAI J.W., Hwang Y.C., Lin S.L., Weng C.H. (2004). Research and application of double-core buckling restrained braces in Taiwan. Proocedings of the 13th World Conference on Earthquake Engineering, Vancouver, B.C., Canada, August 1–6, 2004, Paper No. 2179.
[26] Grant D.N., Blandon C.A. and Priestley M.J.N. Modelling inelastic response in direct displacement based design. Report 2005/3, IUSS Press, Pavia, Italy.
[27] Shinozuka M, Deodatis G. Simulation of stochastic processes by spectral representation. Appl. Mech. Rev, 44. ASME; 1991. p. 191–204.
[28] Vassilopoulou I, Petrini F, Gantes CJ. Nonlinear dynamic behavior of cable nets subjected to wind loading. Struct 2017;10:170–83. https://doi.org/10.1016/j.istruc.2017.03.004.
[29] Solari G, Piccardo G. Probabilistic 3-D turbulence modeling for gust buffeting of structures. Probabilistic Eng Mech 2001;16:73–86.
[30] Carassale L, Solari G. Montecarlo simulation of wind velocity field on complex structures. J Wind Eng Ind Aerodyn 2006;94(5):323–39. https://doi.org/10.1016/j.jweia.2006.01.004.
[31] Liang S, Liu S, Li QS, Zhang L, Gu M. Mathematical model of across-wind dynamic loads on rectangular tall buildings. J Wind Eng Ind Aerodyn 2002;90:201–51.
[32] Freeman, S.A., J.P. Nicoletti, and J.V. Tyrell, 1975, Evaluations of Existing Buildings for Seismic Risk - A Case Study of Puget Sound Naval Shipyard, Bremerton, Washington, Proceedings of the U.S. National Conference on Earthquake Engineers, EERI, pp 113–122, Berkeley.
[33] Fajfar, P. (1998). Capacity Spectrum Method Based on Inelastic Demand Spectra, Report EE-3/98, IKPIR, Ljubljana, Slovenia.
[34] Castaldo P, Tubaldi E, Selvi F, Gioiella L. Seismic performance of an existing RC structure retrofitted with buckling restrained braces. J Build Eng 2021;33:101688.